CHALMERS
UNIVERSITY OF TECHNOLOGY

UNIVERSITY OF GOTHENBURG

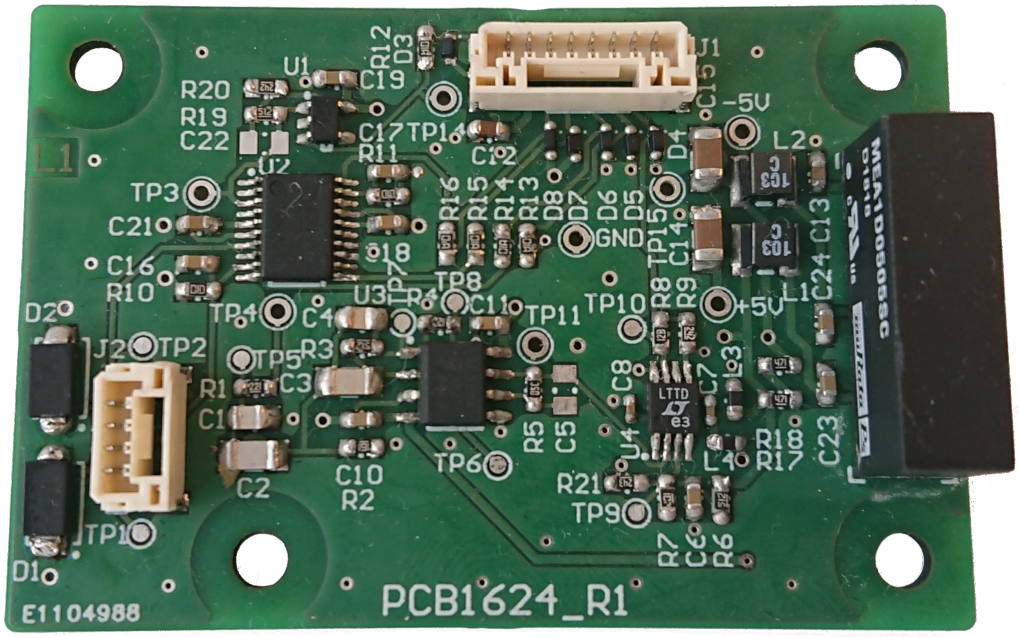

Design and Evaluation of an Ultrasonic Oxygen Sensor for Medical Ventilators

Master's thesis in Embedded electronic system design

Carmen Isop
Andreas Torstensson

Department of Computer Science and Engineering
CHALMERS UNIVERSITY OF TECHNOLOGY
UNIVERSITY OF GOTHENBURG
Gothenburg, Sweden 2019

Master's thesis 2019

Design and Evaluation of an Ultrasonic Oxygen Sensor for Medical Ventilators

CARMEN ISOP, ANDREAS TORSTENSSON

UNIVERSITY OF
GOTHENBURG

CHALMERS
UNIVERSITY OF TECHNOLOGY

Department of Computer Science and Engineering
Chalmers University of Technology
University of Gothenburg
Gothenburg, Sweden 2019

Design and Evaluation of an Ultrasonic Oxygen Sensor for Medical Ventilators
CARMEN ISOP, ANDREAS TORSTENSSON

Supervisor: Lena Peterson, Department of Computer Science and Engineering, Mikael Duvander, i3tex AB
Advisor: Kristoffer Berntsson, i3tex AB
Examiner: Per Larsson-Edefors, Department of Computer Science and Engineering

Master's Thesis 2019
Department of Computer Science and Engineering
Chalmers University of Technology and University of Gothenburg
SE-412 96 Gothenburg
Telephone +46 31 772 1000

Cover: Photograph of the sensor PCB we designed.

Typeset in LaTeX
Gothenburg, Sweden 2019

Design and Evaluation of an Ultrasonic Oxygen Sensor for Medical Ventilators
CARMEN ISOP, ANDREAS TORSTENSSON
Department of Computer Science and Engineering
Chalmers University of Technology and University of Gothenburg

Abstract

Many people are affected by respiratory system diseases and need medical ventilators to help them breathe, often it is also necessary to be able to add extra oxygen to the breathable air meaning it must be possible to measure the oxygen concentration in the ventilator. Right now, the most commonly used sensors for this purpose are electrochemical sensors that are expensive, have slow response-times, not environment-friendly and cannot measure gas flow. As an alternative solution, this thesis proposes a design for an ultrasonic oxygen sensor that is capable of measuring both oxygen concentration and air flow speed, the disadvantage however is that the ultrasonic sensor is non-selective. The design includes a hardware, software and mechanical solution and the tests carried out on the developed system showed that the sensor was multiple times quicker than the reference (electrochemical) sensors. Furthermore, the accuracy of both concentration and flow measurements were within 2.5% of the reference sensor and within the design goals.

Keywords: ultrasonic oxygen sensor, PCB, time-of-flight, flow meter, gas sensors, medical ventilators, engineering, thesis.

Acknowledgements

We would like to thank our i3tex supervisors Kristoffer Berntsson and Mikael Duvander for the discussions and constant support and Carl Erkenstam, Lars Bolander, Ignacio Mancha and Peter Olsson from i3tex for the help with PCB, mechanical and software design.

We would also like to thank our Chalmers supervisor Lena Peterson for her help and feedback on the content and language of the thesis and finally we would like to thank our fellow Chalmers students Kajsa Lenfors and Albin Nykvist for their feedback on the report.

Carmen Isop, Gothenburg, May 2019
Andreas Torstensson, Gothenburg, May 2019

Contents

List of Abbreviations

CMRR	Common-mode rejection ratio
COPD	Chronic obstructive pulmonary disease
CRD	Chronic respiratory disease
DC	Direct current
DMA	Direct memory access
ESD	Electrostatic discharge
FET	Field-effect transistor
FFT	Fast Fourier transform
GBW	Gain-bandwidth product
HP	High-pass
I/O	Input/output
IC	Integrated circuit
IR	Infrared
LC	Inductor-capacitor
LP	Low-pass
MCU	Microcontroller unit
MFB	Multiple-feedback filter
MIS	Metal-insulator-semiconductor
op-amp	Operational amplifier
PCB	Printed circuit board
PWM	Pulse-width modulation
Q factor	Quality factor
RC	Resistor-capacitor
RL	Resistor-inductor
RLC	Resistor-inductor-capacitor
SPDT	Single pole, double throw
STPH	Standardised temperature and pressure, actual humidity
TOF	Time-of-flight
TVS	Transient-voltage-suppression
WHO	World Health Organization

1

Introduction

Many people with various diseases in their respiratory systems or with neurological dysfunctions need ventilators that help them breathe, and in some cases, it is necessary to also add oxygen to the air. To decide when to add oxygen and for what time to add it, oxygen concentration needs to be measured.

The idea of using the acoustic properties of gas mixtures to measure their composition is not new, as the principle can be found patented by General Electric already in their 1942 patent US2283750 [1]. Since then the field of electronics and sensors has evolved. A report on behalf of the United States Air Force in 1987 [2] examined the suitability of a system with an ultrasonic chamber the size of a soda bottle to measure oxygen concentration in airplane oxygen generators. In the past 32 years sensors have evolved further and shrunk to sizes small enough to now be integrated into products smaller than a soda bottle.

The thesis topic was proposed by the company i3tex, which designs medical devices including medical ventilators and wants to investigate the possibility to improve their future devices with an ultrasonic oxygen sensor. Therefore, the work is carried out in cooperation with i3tex.

1.1 Motivation

Chronic obstructive pulmonary disease (COPD) is one of the most common chronic respiratory diseases (CRD). According to World Health Organization (WHO) in 2016 COPD affected 251 million people in the world [3], more than 3 million people die from COPD each year [3] and it is expected to be the fourth most common cause of mortality by 2030 [4]. In addition to other treatments, patients who have low blood oxygen levels need supplemental oxygen. It has been shown that long-term oxygen therapy (also know as supplemental oxygen) can increase the survival rate and improve the life quality of the patients with low oxygen levels [5].

The increasing number of people affected by COPD means that there is an increasing need for devices capable of providing people oxygen therapy. Right now, the most commonly used oxygen sensors in medical devices are electrochemical sensors [6]. However, there are multiple problems with the sensors currently used. The concentration measurement is output as an analog signal which can drift by up to

1% per month, making regular calibration a necessity. The sensors also have a limited lifetime of up to six years, which is further reduced by environmental factors such as temperature and humidity, as well as a shelf life which is limited to six months [7]. After the lifetime ends the sensor is worn out and must be replaced with a new one, which is neither sustainable, nor practical for the user. The sensors also contain lead, which is toxic, and therefore the handling and recycling is further complicated [8]. Due to these factors, along with a high unit price, there is a strong interest in adapting a non-perishable sensor in place of the electrochemical one to reduce the required upkeep of the system.

All the downsides related to electrochemical sensors are the reason for trying to find a new and better solution for measuring oxygen concentration. As mentioned above, acoustic properties have been used for measuring the gas concentration since the 1940s and since then these sensors have shrunk enough to integrate them into medical ventilators.

There already exist some ultrasonic oxygen sensors that are interesting for the purpose on the market, such as the Gasboard7500C [9], which was previously reviewed by i3tex, but they have some significant disadvantages when trying to integrate them into a compact embedded system. The Gasboard7500C has a bulky stand-alone design where it is connected as a complete sensor solution by diverting some of the gas flow to a separate path through the sensor. This feature does make it easy to use in a large system where you want to add another sensor and have it send you the result over a communication bus, but also makes it difficult to integrate into a small system where space comes at a premium and the space to mount an additional sensor and divert gas flow to it from the main path is not available. Therefore, a cheaper and more environment-friendly sensor, which is flexible in layout, can be positioned in the main path, and lean enough for easy integration into an existing system, would be of interest to i3tex, which proposed the topic, for the use in future systems.

1.2 Goals

The main goal of the thesis is to propose the design of an advantageous ultrasonic sensor solution for measuring oxygen concentration and flow speed in a ventilator device.

The first sub-goal is to identify the design requirements of the sensor such as the size, accuracy and response time and how to meet them, as well as how to quantify the performance of the system from parameters such as resolution, response time and sample rate.

In the design phase the goal is to design the hardware of the sensor to meet these requirements set as well as implement a software solution to interpret the signals generated by the sensor as an oxygen concentration. This has to be done while also ensuring compatibility of the design to the existing hardware and software platform so that it can be easily integrated into the ventilator system.

The final goal is to perform test and verification of the device to ensure that the design requirements are met and that the performance can be quantified for the relevant parameters. This step includes designing the test cases for the evaluation of the relevant parameters and requirements. There is also another dimension added to the design phase of the device to facilitate easy testing by ensuring that all signals that may be required are accessible.

1.3 Delimitations

As there already exists a microcontroller (MCU) for the ventilator device which the sensor is to be interfaced to, we do not include the work of selecting and evaluating different MCUs for suitability to control the sensor. The exception would be if performance requirements cannot be reached without more powerful signal processing or more specific hardware capabilities than those of the current MCU, in which case a more powerful or specialised unit might be proposed.

We are limited to what selectivity an ultrasonic sensor offers together with the already present sensors of the ventilator device. We are not looking into improving the selectivity past this point through combining it with the addition of other technologies. Sensors present in the ventilator measure the temperature, pressure and humidity.

The target product of the project is a medical device, therefore, the sensor would require safety certifications which are decisively out of scope for the project. This means that the work will be strictly for performance evaluation and not for clinical use.

1.4 Requirements

The project has a set of requirements dictating what we are trying to accomplish with our sensor design, which we established together with our supervisor at i3tex. There are two types of requirements: those that dictate functionality which needs to be included in the design, and those that dictate the performance we want to achieve. Both types of requirements are directing the design process, but the performance requirements must be evaluated in more detail during testing and are as such to some extent also design goals.

The complete requirements of the sensor are as follows:

- The total sensor volume should be no more than 50 cubic centimeters, comparable to current ventilator sensor volume.
- The operating temperature should range from 5°C to 40°C.
- The operating humidity should range from of 5 to 95 %, but does not include condensation.
- The operating pressure should range from 700 to 1100 hPa.

- The sensor should be able to measure flow in both forward and reverse direction (to and from the ventilator).
- The oxygen measuring accuracy should be in line with the ISO 80601-2-55:2018 standard of ±(2.5% + 2.5% of gas concentration).
- The flow rate should be measured with the same accuracy of ±(2.5% + 0.5% of the measurement range), comparable to current ventilator flow sensor.
- The response time for oxygen concentration should be as short or shorter than that of the reference sensor(s).
- The response time for flow rate should be 1 ms or less.
- The flow rate measurement should be able measure flows with a rate of 400 litres per minute.
- The sensor should operate from the voltages available in the system: 3 V, 5 V and 24 V.

1.5 Method

The thesis work starts with a theoretical pre-study, which describes the principles of how ultrasonic sensors can measure oxygen and gas flow, and explores competing sensor technologies in oxygen concentration and flow measuring. The research part is important for choosing the best path to follow when considering how the sensor should be designed.

Our two main areas of research were:

- the theory behind measuring oxygen content and gas flow acoustically through ultrasound including the description of the algorithms required and any advantages and limitations of the method;
- the market availability of small oxygen sensors to gather an overview of different kinds of suitable sensors currently available;

System design consists of hardware and software design, where the hardware design covers the design choices of the circuit of our sensor, including schematic and printed circuit board (PCB) design. The software design covers controlling the interface between the sensor circuit and the MCU as well as the implementation of the algorithms to calculate the oxygen concentration from the resulting sensor output.

There is also some mechanical design work in deciding the sensor geometry and designing a test structure where the transducers can be mounted to provide a controlled test environment for measurements to take place. The final part of the thesis work is testing the sensor and then whole system - our part integrates with the existing system to establish accuracy versus factors such as temperature, humidity, air flow and sample rate.

1.6 Ethical aspects

As any clinical testing or certification is outside the scope of the project, there are no associated immediate risks of clinical use. However, as a future goal of a successful project would be moving towards certifying the device for clinical use, there is an ethical consideration in evaluating the performance of the device accurately. Additionally, the risk of malfunction and its dangers also have to be considered.

1.7 Thesis outline

This introductory chapter is followed by the Ventilators and Gas Sensors chapter, which first gives some background on ventilators and introduces other types of gas sensors with a primary focus on those used in ventilators. Then the chapter introduces the principles of ultrasonic gas sensors with the different attributes of ultrasound which can be utilised, their strengths and weaknesses and the equations behind the time-of-flight method we have chosen to use.

The Amplifiers and Filters chapter introduces the basic theory behind the different electronic parts of our system, so the reader will have a clear idea of possible design options before going into the System Design chapter.

The System Design chapter covers the development process of the sensor system, describing the system first from an overview perspective to then delve deeper into how the specific components were selected and how the final design was established.

The Design Implementation and Test Results chapter then describes the final system design implementation starting with the PCB design and software implementation and concluding with all the necessary test results.

Finally, the Conclusion chapter begins with a discussion of the results, the advantages and disadvantages of the developed device and possible improvements. The chapter ends with a summary of the whole work from where we started and what results were obtained.

2

Ventilators and Gas Sensors

This chapter first reviews the history of medical ventilators and how these devices have evolved, after that different gas sensors that are interesting in the context of ventilators are introduced. The chapter continues with the introduction of ultrasonic gas sensors and their main working principles and the chapter is concluded with a part on flow sensors.

2.1 Ventilators

Mechanical ventilation has roots dating back to the late 17th century with the exploration of the mechanics of the respiratory system performed by Mayow [10]. The Royal Humane Society of England supported the use of bellows as a form of positive pressure mechanical ventilation in the 18th century and the method was widely used until falling out of fashion in the mid-19th century after it was criticized by a J. Leroy [10]. In the early 20th century the company Drägerwerk manufactured a resuscitation device for pumping air or oxygen into the lungs of hypoxia victims, but the device seems to have seen no use as a ventilator [11], [12].

During this period and up until the 1950s the main form of mechanical ventilation was instead the negative pressure cabinet ventilators, or "iron-lungs", used in the treatment of polio patients, the first of their kind described in 1876 by Woillez [10], [13]. The cabinet ventilator operates by enclosing the patient with only the head exposed and the machine creates a negative pressure around the body by pumping air out, to inflate the lungs, rather than forcing air down the airways by positive pressure. This means that the machines are large and the patients are rendered virtually immobilised in the machine. An open and unoccupied ventilator is shown in Figure 2.1, which also makes the size of the machine apparent.

The beginning of modern positive-pressure ventilation, outside of anaesthesia [13], was seen in 1952 as the Blegdam Hospital of Copenhagen ran out of cabinet ventilators during a polio epidemic [12]. This shortage prompted the hospital to manually perform positive-pressure ventilation on the patients with the help of 1400 medical students [10]. When patients treated by this practice turned out to suffer significantly lower mortality rates than those treated by cabinet ventilators, the development of positive-pressure ventilators as well as manually operated re-inflating bags for assisted breathing begun [13].

Figure 2.1: Cabinet ventilator, also known as an "iron lung". The enclosure, bed and head hole (left) visible. From [14]. PD-USGov-HHS-CDC.

The first modern portable ventilators emerged in the mid-50s with the French RPR ventilator developed by Rosenstiel, Pesty and Richard, designed for artificial ventilation during transportation of patients in 1955, and the Bird Mark 7, developed by Forrest Bird in the US in 1956 as the first low-cost and mass-produced device [12], [13]. The Mark 7 was followed by the Mark 8 which is pictured in Figure 2.2. These devices were mechanically powered by compressed breathing gas coming from pressurised bottles, but modern devices utilise electrically powered compressors to pressurise ambient air and use digital control systems for regulation [12].

In these devices parameters such as flow rate, temperature and humidity are measured by sensors as part of the control system and, in the case of oxygenated ventilation, so is the resulting oxygen concentration of the outgoing air. There are multiple different types of sensors used to monitor the oxygen concentration, with their specific advantages and disadvantages, but some common ones are electro-galvanic cell-based sensors [16]–[18], paramagnetism-based sensors [18]–[20] and ultrasound-based sensors [21]–[23].

2.2 Gas sensors

Apart from ultrasonic gas sensors, there are many other types of gas sensors available on the market and even more explored in research based on wildly varying principles. Limiting the scope to sensor types that are capable of detecting oxygen concentration and have some market presence, we make the field smaller. This section introduces some of those sensors which we found interesting in the context of ventilators, even

Figure 2.2: The Bird Mark 8 medical respirator. From [15]. PD-CC0.

if we have found no evidence of ventilators that utilise them.

Ultrasonic sensors can be used to measure oxygen concentration and are used in ventilators, but they have their own in-depth section in Section 2.3 and are therefore not a part of this section.

2.2.1 Optical sensors

Absorption-based optical sensors measure the change in intensity of the optical signal due to the presence of their detected gas. For gases with unequal atoms such as carbon dioxide this can be done in the infrared (IR) spectrum by detecting the gases strong IR absorption [24]. But for oxygen there is only weak absorption in the near IR band, which requires narrow-band optics such as lasers for detection [25]. An alternative method for absorption-based detection of gases is with a reagent compound in the optical path, of which the absorbance changes as it reacts with the detected gas [26]. This way gases without strong absorption can also be detected, but it requires a reagent compound which reversibly reacts with the specific gas that is being detected and exhibits an optical response doing so [27].

Luminescence-based sensors utilise luminescent (fluorescent, phosphorescent) dyes which are excited by an optical signal [27]. Normally as the dye exits the excited state it emits a photon carrying the excess energy away, but when a molecule of the gas being detected by the dye collides with it this energy is instead transferred to the molecule resulting in no emitted photon. This way the gas concentration can be measured by its inverse correlation to the number of photons re-emitted by the dye.

2.2.2 Metal oxide semiconductor sensors

There exist five types of semiconductor gas sensors, with transducers based on diodes, metal-insulator-semiconductor (MIS) capacitors, MIS field-effect transistors (FET), oxygen concentration cells and resistors [28]. But, as of 2013, only resistor-based oxide semiconductor gas sensors are well established on the market. They sense gases present as a heated semiconducting oxide film, or bead, reacts with specific gases either on surface or in bulk leading to a change in the oxide's resistance [29].

2.2.3 Electrochemical sensors

At their core electrochemical gas sensors are cells where specific gases are electrochemically oxidised or reduced, which creates an electrical potential or current across the cell proportional to the present gas concentration [24], [26]. Common for the operation of these sensors is that the gas reacts with the sensor: either it moves through the sensor due to a concentration gradient or pumping bias, or it acts as a fuel cell where the gas reacts with an anode to create a current [25], [30]. The sensors can be either potentiometric, generating a voltage as the sensing signal, or amperometric, generating a current [26].

Regardless of the sensing signal, electrochemical cells usually consist of at least two electrodes, one for the sensing side and one for the reference side, and an electrolyte in between. Potentiometric sensors have an advantage in the output signal being independent from the size of the sensor, allowing for small sensors to be created without lowered output signal, but their concentration response is logarithmic which can limit their suitability to certain applications [31]. In high-temperature potentiometric sensors, the electrolyte often is a ceramic solid [24], [26].

One of the most well-known oxygen sensors, the lambda sensor, used in cars to monitor the oxygen content of the exhaust to control the air-fuel mixture to maximise the combustion efficiency, is a potentiometric electrochemical sensor [32]. It was first introduced to series production cars by car manufacturer Volvo in 1977 after being developed for the application by Bosch in the preceding decade [33], [34]. It is a cell made out of an oxygen-ion-transporting ceramic electrolyte, yttria-stabilised zirconia, with platinum electrodes, where the oxygen concentration difference of the two sides of the cell creates a voltage potential across the electrodes as oxygen is ionised and travels through the electrolyte [29]. But for this ceramic to gain its oxygen transporting properties it needs to be heated to above 300°C which is a good match to the exhaust system of a combustion engine but less so to many other environments. The ionisation and transportation of oxygen also means that this kind of sensor is not able to measure passively without reacting with the gas it is sensing.

While not originally a gas-phase sensor, Leland Clark invented one of the most well-known electrochemical amperometric oxygen senors for the measurement of blood-oxygen levels [31]. The sensor known as a polarographic sensor, or the "Clark

oxygen electrode", consists of an electrolytic solution with two electrodes and a membrane to the environment through which oxygen can diffuse into the solution and the sensor then generates a current signal, proportional to the amount of diffused oxygen when biased with a driving voltage. This principle has been developed into gas-phase sensors for O2 and NO2 amongst others [31]. While not requiring the high temperatures of the lambda sensor, these sensors are sensitive to environmental change and for a stable output they generally require compensation for temperature and humidity changes.

Electro-galvanic oxygen sensors with consumable anodes are an amperometric type of sensors similar to the polarographic, but instead of being externally powered, they function as fuel cells where the reduction of the oxygen being measured generates the power of the current signal [25], [26]. Just like regular fuel cells and batteries, this kind of sensor has a limited lifetime as it runs on a chemical reaction that will eventually run out of available fuel. As the reaction speed depends on the oxygen available to the sensor the life becomes shorter in high-oxygen environments. Other environmental factors such as humidity and temperature can also be factors with some sensors being limited to operate between 10 and 40 °C [7], [25]. Currently lead anodes is a common choice in this kind of sensor [8], but with the RoHS EU-Directive ending the use of lead in detection instruments in 2024 research has been directed into finding other suitable anode materials and such sensors have appeared on the market [35].

2.2.4 Paramagnetic oxygen sensors

Paramagnetism, attraction to magnetic fields, sets oxygen apart from the other gases commonly found in air which all are diamagnetic, repelled by magnetic fields [36]. This property can be utilised to create a sensitive and highly selective oxygen sensor. An early design of a paramagnetic sensor, from the 1940s [37], has a sensing body which consists of two nitrogen filled glass spheres connected by a rod. This sensing body is suspended by the midpoint of the rod in a strong magnetic field [38]. When the sample gas flows through the sensor, oxygen (attracted to the magnetic field) will impose an uneven force on the the sensing body which causes it to rotate. The sensor then measures either the displacement, or the force required to counteract displacement, of the sensing body to calculate the amount of oxygen present in the sample. This design does however have several weaknesses in being fragile and sensitive to shock, vibration, tilt as well as flow variations while also being expensive [38].

Newer sensors utilising switched magnetic fields to measure concentration in gas mixing have been designed and are used in medical oxygen monitors and ventilators [39]. These are less mechanical in their construction and therefore less fragile, but they do instead require the concentration measurement to be performed at the mixing point of two gases [20].

2.3 Ultrasonic gas sensors

Ultrasonic sensors use ultrasonic wave propagation to measure physical or chemical variables. While the main ultrasonic sensors are divided into two categories, viz. propagation-path sensors and distance-sensors, ultrasonic gas sensors are all in the first category. Propagation-path sensors decode the changes in the wave propagation to measure the temperature, pressure or gas concentration of the medium; the changes usually observed are in the propagation time, signal phase or attenuation [40].

Ultrasonic sensors have excellent long-term stability and therefore long lifetime. They also have a low power consumption and they do not cause secondary pollution like some alternatives do, making them a more environment-friendly option. Another advantage more specific to gas sensors is that measuring gas properties can be combined with measuring the gas flow velocity which makes it possible to use flowmeters also as gas analysers [41]. Ultrasonic gas sensors also have high accuracy, high linearity and quick response time and they work in wide variety of gases [40].

Disadvantages, however, are that ultrasonic gas sensors have low selectivity, so they can only be used on gases that have known composition. This is because only the changes in sound wave propagation times are measured by the sensor, the rest of the information for composition calculations needs to be known or measured separately (more on how the composition is calculated in Section 2.3.1). Furthermore, the sensors are also limited to binary and pseudo-binary gas mixtures, as more information is needed to determine the composition if the mixture consists of more than two gases [41].

Air and oxygen are considered a pseudo-binary gas since the composition of air is known and quite constant and is almost entirely made up of oxygen, nitrogen and argon. Unless the air is dry it does also contain a variable fraction of water vapour, but by measuring the humidity this can be accounted for in the calculations [42].

There are three main methods for measuring the gas properties using ultrasonic waves – speed of sound, attenuation and acoustic impedance [43]. The next sections describe their working principles and the advantages and disadvantages each method has.

2.3.1 Speed of sound

This method uses the speed of sound and is the most popular and the most studied sensing method for ultrasonic sensors. The most common way to measure the speed of sound is by using the time-of-flight (TOF) method. TOF is based on measuring the travel time, t, of an ultrasonic wave at a given distance d, which is usually the distance between the transmitter and the receiver [43]. The TOF is then used to calculate the propagation velocity of the ultrasonic wave as

$$c = \frac{d}{t} \tag{2.1}$$

and from that the gas concentration can be reached [41].

To find the formula for calculating the gas concentration, we first go back and find the formula for the speed of sound. According to the Newton-Laplace equation [44]

$$c = \sqrt{\frac{K_s}{\rho}} \tag{2.2}$$

the speed of sound depends on the bulk modulus (K_s) and the density of the matter (ρ). If we combine this equation with the bulk modulus ($K_s = \gamma P$) and ideal gas law ($P = \rho \frac{R}{M} T$) formulas [45], we get the equation

$$c = \sqrt{\frac{RT\gamma}{M}}, \tag{2.3}$$

where R is the gas constant (8 314472J/molK) [44], T is the temperature of the gas, γ is the specific heat ratio and M is the molecular weight. For the binary gas, the molecular weight is calculated using this formula [46]

$$M = X_1 M_1 + X_2 M_2 = X M_1 + (1 - X) M_2, \tag{2.4}$$

and the specific heat ratio using this expression [46]

$$\gamma = \frac{X_1 C_{p1} + X_2 C_{p2}}{X_1 C_{v1} + X_2 C_{v2}} = \frac{X C_{p1} + (1 - X) C_{p2}}{X C_{v1} + (1 - X) C_{v2}}, \tag{2.5}$$

where X is the mole fraction, C_{vi} the heat capacity at constant volume and C_{pi} the heat capacity at constant pressure of a specific gas component. For oxygen mixed with air, C_{v2} and C_{p2} are the heat capacities of the air mixture excluding the oxygen which is represented in C_{v1} and C_{p1}.

Combining (2.3), (2.4) and (2.5) we get the formula for the speed of sound in binary gases

$$c = \sqrt{\frac{RT \frac{X C_{p1} + (1-X) C_{p2}}{X C_{v1} + (1-X) C_{v2}}}{X M_1 + (1 - X) M_2}}. \tag{2.6}$$

From (2.6) it is possible to derive the formula for the concentration of one of the gases:

$$X = \frac{\frac{T}{c^2} R (C_{p1} - C_{p2}) - K_2 + \sqrt{(K_2 + \frac{T}{c^2} R (C_{p2} - C_{p1}))^2 + 4 K_1 (\frac{T}{c^2} R C_{p2} - M_2 C_{v2})}}{2 K_1}, \tag{2.7}$$

where

$$K_1 = (M_1 - M_2)(C_{v1} - C_{v2}) \tag{2.8}$$

and

$$K_2 = (M_1 - M_2) C_{v2} + M_2 (C_{v1} - C_{v2}). \tag{2.9}$$

However, there are also papers [47] that calculate the specific heat ratio for binary gases the same way as the molecular weight is calculated, therefore using

$$\gamma = X_1\gamma_1 + X_2\gamma_2 = X\gamma_1 + (1 - X)\gamma_2. \tag{2.10}$$

This means that the formula for calculating the concentration of one of the gases is

$$X = \frac{RT\gamma_2 - c^2 M_2}{c^2(M_1 - M_2) + RT(\gamma_2 - \gamma_1)}. \tag{2.11}$$

Comparing (2.6) and (2.11) using Matlab to sweep a mixture from pure oxygen to normal air, we found that the difference between them across the possible concentration span is only 0.02 to 0.03 %. This is so small a difference that even if (2.6) happens to be more accurate, the calculation complexity is so much higher for (2.6), that the lower calculation difficulty of (2.11) will most likely be preferable when using an MCU to perform the conversions in real time.

The main advantage of TOF is that it is very simple; there are only two transducers needed and the concentration can simply be calculated from the measured information. It is also the most studied method out of three described in this paper [43]. These are the reasons why it is the most common solution.

2.3.2 Amplitude attenuation

The attenuation refers to the energy that is lost when an ultrasonic wave travels through the gas. It has been proven that the amplitude attenuation is dependent on the gas the wave is passing through. This phenomenon makes it possible to detect gases and calculate their concentrations [43].

Petulescu et al. [48] write that the classical sound attenuation is caused by transport phenomena (like heat conduction, viscosity and diffusion). However, the reason for non-classical absorption is the thermal relaxation. When there are no perturbations in the gaseous medium, the internal degrees of freedom of the molecules are thermalised, meaning that at constant temperature, the gas is in a thermal equilibrium. However, launching an acoustic wave in the gas breaks the equilibrium as the internal degrees of freedom that are activated by the molecule collisions have to relax the acoustic temperature. This causes an increase in absorption of sound.

While the attenuation caused by heat conduction, viscosity and diffusion are well understood and can be calculated when necessary values are known, the attenuation caused by relaxation is much more complicated to calculate [49].

The system setups for attenuation measurements are also more complicated compared to those of the TOF method. Ejakov et al. [49] used four transducer pairs and were able to measure attenuation accurately in pure gases and binary mixtures. Petulescu et al. [48] used two pairs of transducers and concluded that this had some limitations because of only having two sensing paths. Furthermore, attenuation

measurements require careful calibration and it is a less robust method which can be affected by turbulence, particles or droplets in the gas [41].

There are multiple reasons as mentioned above why the attenuation method is not used in commercial sensors, however, Petulescu et al. [48] concludes that "...combining sound speed and attenuation measurement in a simple sensor offers the potential to identify and quantify the gases making up a multicomponent mixture."

2.3.3 Acoustic impedance

The third parameter used for ultrasonic gas sensing methods is acoustic impedance. The impedance is given by equation $Z = \rho C$, where ρ is the gas density and C is the speed of sound. Therefore, it is usually used to determine gas density, meaning it is not suitable for our application. Furthermore, the measurement of the acoustic impedance of a gas is very difficult, so this method is not being widely used [43].

2.4 Ultrasonic gas flow meters

Flow meters measure the velocity of a fluid and the flow can be measured both in volumetric and mass flow rates. Ultrasonic gas flow meters use ultrasonic waves to measure gas flow. Flow meters are used in different industrial processes, medical devices (respirators, anaesthesia machines), internal combustion engines, gas heating systems and so on [40].

This technology has multiple advantages over other flow meters, as its system contains no moving parts and it does not create an additional pressure drop unlike turbine or differential pressure based sensors [50]. It is also insensitive to gas composition fluctuations and allows bi-directional flow measurement and provides information about speed of sound that can be used in other applications. Finally, it has a short response time which makes it possible to measure transient or pulsating flows. These advantages can also reduce the installation and maintenance costs [51].

There are two main measuring principles for ultrasonic flow meters – Doppler shift and transit-time. Doppler method depends on scattered particles, as it measures the particle velocity using the Doppler effect. A transducer emits an ultrasonic wave and the wave is partly backscattered from the particles and the same transducer receives the backscattered wave. The movement of the particle causes a frequency shift in the wave proportional to the particle velocity [52]. However, the Doppler method usually suffers from limited accuracy and the dependency on scattered particles like impurities in the gas [40].

The transit-time method, however, has high accuracy and very short time delays making it the most widely used technique for flow measuring. The method works by measuring the time of flight of the ultrasonic wave between two transducers, as time required for the wave to travel depends on the distance L between transducers,

flow velocity v, the speed of sound c and the angle α between the direction of flow and the direction of the wave propagation [40].

To calculate the flow velocity without having to measure the speed of sound in the medium, the difference of the reciprocals of the propagation time in both directions is needed, therefore the formula for calculating the speed of flow is [40]

$$v = \frac{L}{2\cos\alpha}(\frac{1}{t_2} - \frac{1}{t_1}) = \frac{L}{2\cos\alpha}(\frac{t_1 - t_2}{t_1 t_2}), \tag{2.12}$$

where t_1 and t_2 are the propagation times.

By multiplying the flow velocity v (m/s^2) with the area of the flow a (m^2) and the conversion factor 60 000 we obtain the volumetric flow (l/min) V

$$V = v \times a \times 60000. \tag{2.13}$$

Sometimes an additional factor k to compensate for profile effects in the sensor is required as well [41]. The flow velocity can then be converted to a standardised temperature and pressure, actualy humidity (STPH) value through [53]

$$V_{STP} = V\frac{P_x T_s}{P_s T_x}, \tag{2.14}$$

where P_s is the standard pressure, 101.3 kPa, T_s the standard temperature, 294.25 K, and P_x, T_x the pressure and temperature at the time of the velocity measurement. This normalisation to standard litres per minute allows the measured flow to be related to other measurements taken under different circumstances.

3

Amplifiers and Filters

This chapter aims to give an overview of the theoretical background behind the most important design decisions for the system. We start off with introducing amplifiers where we focus on operational amplifiers (op-amp) and the core principles and specifications behind their operation, along with the comparator as a special case of the op-amp. Then we introduce the filter design and all the different filter classifications.

3.1 Amplifiers

An amplifier is a device which acts as a multiplier of one or more aspects of a signal, such as voltage or current, ideally increasing their magnitude linearly by a set factor without being affected by other factors such as frequency [54]. In place of an ideal amplifier, negative feedback (as first described by H. S. Black in his 1934 paper "Stabilized Feed-Back Amplifiers" [55]) is usually used to limit the gain to a well-defined value below the amplifiers maximum gain, this lower gain is then also achievable across a wider frequency span.

Two common applications of amplifiers are signal and power amplification. They both benefit from the same amplifier attributes but the priorities somewhat differ. In signal amplification the goal is to maintain the relative shape of the signal, with minimal distortion, typically with well-matched input impedances to minimally affect the input signal. Power amplification on the other hand aims to add power to the signal to drive a load, sometimes with less care for distortion, through minimising the output impedance.

3.1.1 Transistor circuits

It is completely viable to construct amplifiers out of discrete transistors and they can compete with and outperform other solutions such as op-amps. However, when constructing signal amplifiers this way the number of components required quickly rises and the complexity can increase further by having to use gain-matched transistors [56]. Power amplifiers are much simpler if there is no major distortion requirement or the input is for example a square wave. Then simple single-transistor circuits workign with with a pull-up or pull-down resistance can be used as done

by Psoc et al. [57] for ultrasonic transducers. The resistor will, however, then act as a series resistance to the transducer for operation in one direction and a parallel load on the transistor in the other as shown by the simplified schematics of Figure 3.1. This limits the delivered power with a high resistance or increases the power consumption with a low resistance.

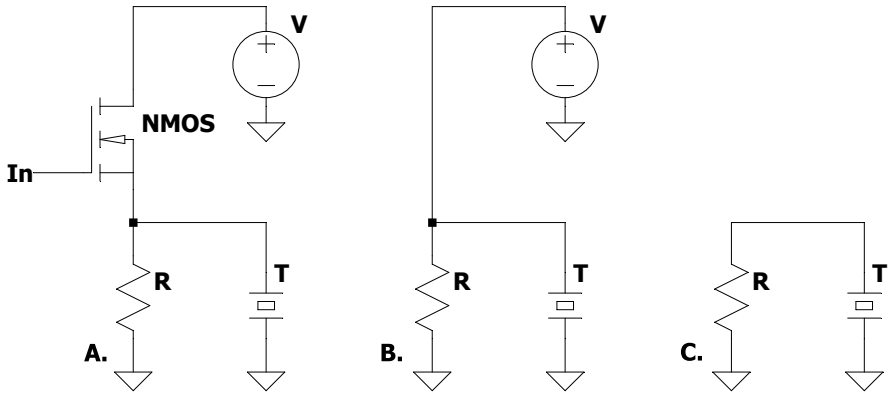

Figure 3.1: A simple transistor based transducer schematic A. is shown together with its two operating states when using the transistor as a switch, B. when the transistor is conducting and C. when the transistor is not conducting. In B. the transducer T and the resistor R make up a parallel load on the voltage source V increasing the power consumption. In C. the resistance R instead acts as a serial load on the transducer T, limiting the discharge current.

3.1.2 Operational amplifiers

Op-amps offer a simpler design and lower component count alternative to building amplifiers out of discrete transistors through implementing such circuits in an integrated circuit format [58]. They are two-input, usually single-output devices and multiple ones are often packaged together in a single package. Their core function, as described by The Art of Electronics' two "Golden Rules" [56] of op-amps with external negative feedback, is that the output will move to minimise the voltage difference between the inputs and there is no current drawn through the inputs. They have very high gain when moving the output in reaction to the input, which means that a slight difference on the input will swing the output hard but also that adding a set amount of negative feedback will turn the op-amp into a fixed-gain amplifier. This can both be achieved with an inverting or a non-inverting output depending on how the signal and feedback is connected to two the input terminals, as shown in Figure 3.2.

Being analog integrated circuits, and not ideal components, op-amps also have long specifications dictating how they perform in reality. The most central in many applications is the gain-bandwidth product (GBW). It is the product of the frequency and the gain of an open loop amplifier (without feedback) and describes the linear behaviour of the gain. It can be used to calculate the achievable gain at frequencies below the GBW through dividing it by the frequency [59]. Related to the GBW

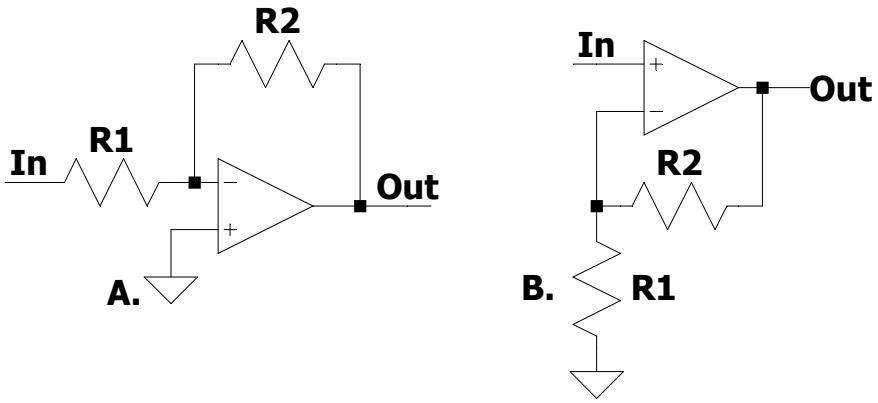

Figure 3.2: Two of the simplest op-amp circuits, the inverting (A) and non-inverting (B) amplifier. The gain is set by ratio of R2 over R1, plus 1 for circuit (B).

is the slew rate, usually given with the unit V/µs, which designates how fast the output moves in reaction to a step change of the input signal [56]. Approaching this limit pushes the op-amp into non-linear operation and leads to output distortion. The output turns into a more and more triangular wave of decreasing amplitude as it fails to keep up with the input signal.

When designing a pure amplifier the GBW directly limits the maximum gain that can be achieved at a frequency, but for filters it is often recommended have a GBW of at least

$$GBW = 100 \times gain \times f_{co} \tag{3.1}$$

where f_{co} is the filter cutoff frequency, to minimise the gain error to below 1 % [59]. There are claims that this formula is much too conservative [60] for most applications and it sometimes also includes the filter's quality factor (Q factor) as an additional factor [61], but it is a useful starting point when narrowing down the suitable op-amps for a design.

Even if the golden rules of an ideal op-amp state that there is no current drawn on the input, there is an input bias current drawn in reality. In many cases it is very small in the µA down to fA range [62]. But this bias current can still manifest itself as a load on the input signal leading to a lowered signal level or on the amplifier output leading to a direct current (DC) output offset, depending on where the current ends up being drawn from [56]. Additionally there is also the input offset voltage, often in the single mV range, which due to imbalance in the input stages leads to zero output happening at a slight difference between the inputs rather than when they are exactly equal [59]. This will also lead to a DC offset of the output in relation to the feedback networks resistance, where it grows with impedance. Some op-amps have specific terminals to allow compensating the offset voltage. Some care has to be taken to ensure that the effects of these non-idealities can not grow too large in each particular design.

In non-inverting amplifiers there is also the common-mode rejection ratio (CMRR) which dictates to which degree the amplifier can reject a common voltage on both inputs [56].

3.1.3 Comparators

Comparators are a special case of the op-amp, purpose made to be used without feedback, that output either a high or a low voltage based on the differential polarity of the inputs – they compare the inputs [56]. Being purpose made for comparisons, they often have additional features suitable for comparison applications such as separate input and output ranges or latched outputs [63] and they are usually used with input hysteresis to prevent unstable outputs. An important behaviour of comparators is that their comparison delay decreases with overdrive of the input signal past the reference point [56]. The recommended overdrive voltage is often in the few millivolts range and the delay increases exponentially as the input differential falls below the overdrive voltage [63]. This means that it is advisable to design circuits where the expected input differential reaches well past the overdrive voltage.

3.2 Filters

Filters are important parts of almost all electronic systems, as they make it possible to separate the wanted signal from the noise which is present in every system. Filters are divided into two sub-categories: analog and digital filters. Analog filters are built of analog components and are capable of filtering analog signals, while digital filters are usually embedded in chips like an MCU or a digital signal processor and therefore can only filter digital signals. Another way to divide filters into two categories is discrete-time and continuous-time filters, with the first one filtering signals that are discrete in time (certain number points in time) and the other one filtering signals that are continuous in time (infinite points in time). This section is focusing on continuous-time analog filters, as in our system the filtering is done in the analog domain.

Filters are categorised by the frequencies they are letting through: high-pass (HP), low-pass (LP), band-pass, band-stop and all-pass. In addition to this, analog filters can also be divided into multiple classes depending on different characteristics: implementation - active or passive, response - Bessel, Butterworth and Chebyshev, topology - multiple-feedback, Sallen-Key, State variable, biquadric and Cauer. Next, different filters are described and compared to give a better idea of what characteristics they have and what should be considered when choosing a filter.

3.2.1 Filter responses

An ideal brick-wall filter would eliminate everything outside the pass-band, meaning for a LP filter it would remove everything above cut-off frequency and for a HP

filter everything below cut-off frequency, meanwhile perfectly passing everything through in the pass-band. However, with real filters this is not true. Steep roll-off usually means having ripple in the pass-band and flat pass-band is accompanied by less steep roll-off [64]. Therefore, it is important to choose the best filter response according to the systems requirements. Next, the three most common filter responses – Butterworth, Chebyshev and Bessel are introduced.

Butterworth
The Butterworth filter has no ripple in the passband and is because of this often called a maximally flat filter [65]. However, as a drawback, it has a relatively wide transition region from passband to stopband. Otherwise, the Butterworth filter is considered a good all-round performer, with moderate overshoot and ringing and a more linear phase response than some other filters. At the cut-off frequency, the attenuation is at -3dB with an additional $-20\,\mathrm{dB}$ per decade per pole after the cut-off frequency [64].

Chebyshev
The main selling point for the Chebyshev filter is the steep roll-off, which is steeper than that of the two other types. The trade-off for the roll-off is ripple in the passband, which is the reason for it not being suitable for use in certain systems. The filter also has more ringing than the Butterworth filter. The cut-off frequency is defined as the frequency where the response falls below the ripple band, and depending on the order of the filter, the cut-off frequency can be at 0 dB (even-order) or at –(ripple) dB (odd-order). The reason for this difference is that for even-order filters the ripple is above 0 dB gain, while for odd-order filters it is below 0dB gain. The attenuation in the transition band is also not defined by a uniform value per decade [64].

Bessel
The main advantage of the Bessel filter over the others is that it has a constant group delay in the passband, meaning that it can preserve the shape of the wave very well; it also has minimal ringing. The constant group delay is perfect for square wave signals and other signals with multiple frequency components, as it causes no overshoot because all the frequencies are delayed by the same amount of time. However, as a trade-off it has the least steep roll-off out of the three filters mentioned. The cut-off frequency for the Bessel filter is the same as it is for Butterworth at -3dB [64], however, like with Chebyshev filter, the attenuation on the transition band is not defined by a uniform value per decade.

Figure 3.3 shows the frequency responses and group delays of all three first-order filters with cut-off frequency at 40 kHz, while Figure 3.4 shows the same for the second-order filters. As it can be seen, for the first-order filter there is no difference in the frequency response or group delay among the three different types. For the second-order, however, there are clear differences confirming the characteristics described above.

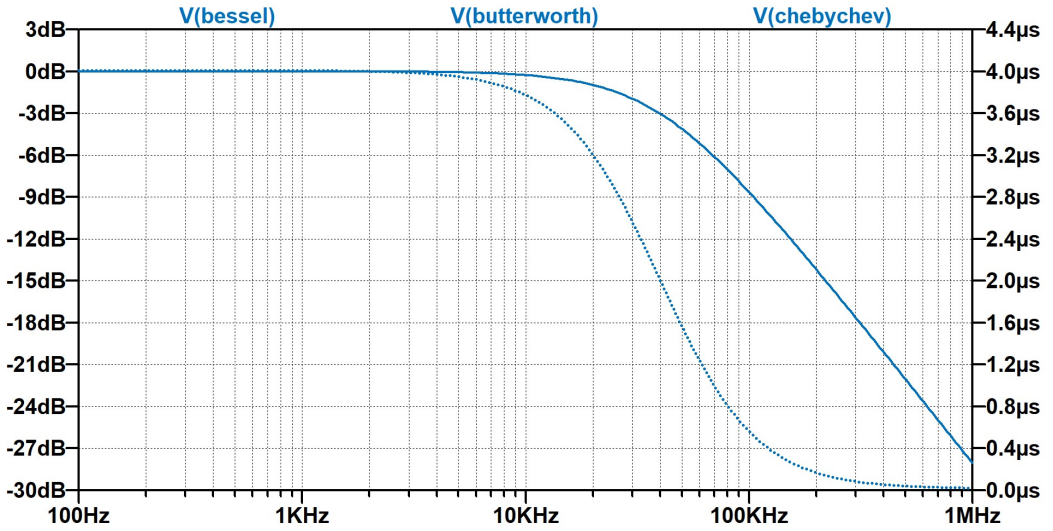

Figure 3.3: Frequency response and group delay graph for first-order Butterworth, Chebyshev and Bessel filters. All three are the same, which is the reason why all are coloured blue.

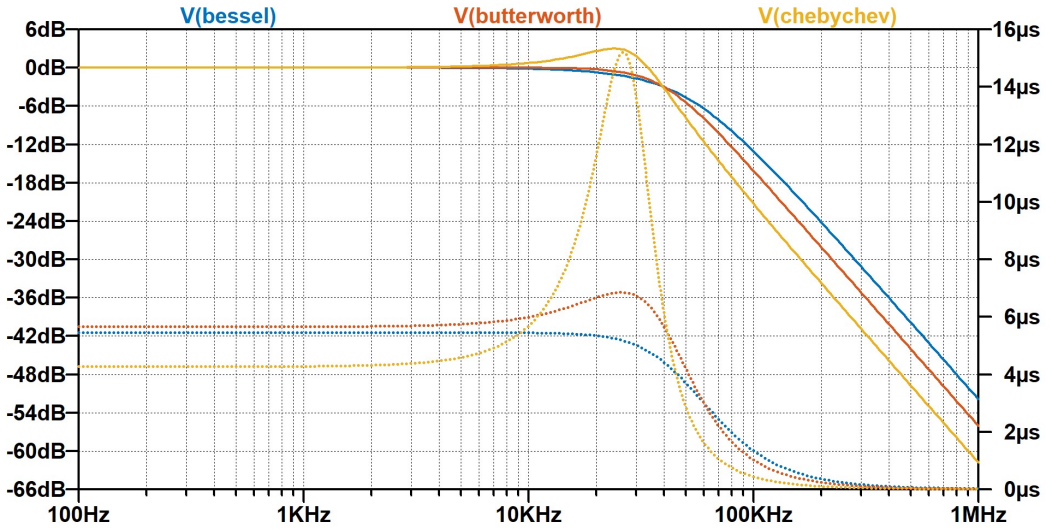

Figure 3.4: Frequency response and group delay graph for second-order Butterworth, Chebyshev and Bessel filters.

3.2.2 Filter implementation

Depending on what components are used for building the filters, they are divided into active and passive filters. As the name indicates, passive filters are built using only passive components, meaning they do not depend on an external power supply and they cannot amplify the signal, as they use no active components. In contrast active filters include both active and passive components, op-amps usually being the active components. Active filters require an external power source and amplify the signal [65].

Passive filters
As mentioned above passive filters are made of passive components only, meaning they are built combining resistors, capacitors and inductors depending on the type of filter. For a given transfer function passive filters need the lowest number of components and are therefore considered the simplest filters. The smaller number of components and no need for a power supply are some of the advantages passive filters have. The other advantages are that as there are no op-amps. The filters are not restricted by op-amps bandwidth limitations which means that the filters work well at very high frequencies [65]. It is also much easier to scale the passive filters to large signals (large current or voltage levels) and the noise generated from passive filters is only thermal noise, meaning it is easier to decrease the noise levels with good design.

However, there are also some disadvantages that make the passive filters unsuitable for certain applications. Most importantly, they cannot provide signal gain and are difficult and time-consuming (for large quantities) to tune because of the component inaccuracies and standard values. Finally, designing complex high-order passive filters can end up being difficult and time-consuming [65].

The most common passive filters are RC (resistor-capacitor), RL (resistor-inductor), LC (inductor-capacitor) and RLC (resistor-inductor-capacitor) filters. Figure 3.5 shows the LP filter circuits for them.

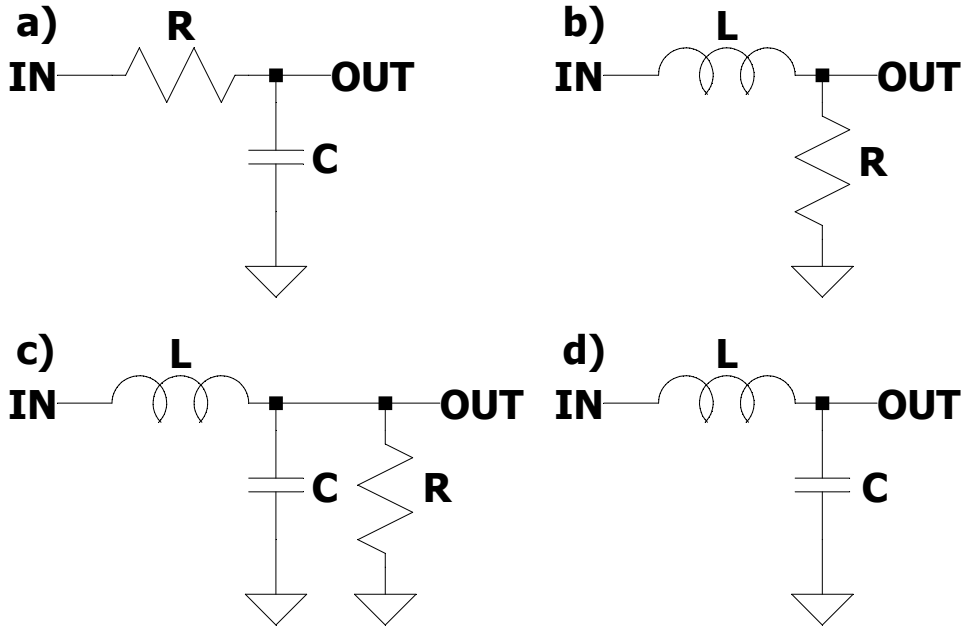

Figure 3.5: Circuit diagrams for RC (a), RL (b), RLC (c) and LC (d) LP filters.

Active filters
Active filters have amplifying parts in addition to resistors and capacitors and can therefore also amplify the signal while filtering it. Resistors and capacitors are placed in amplifier's feedback loop to get the desired filter characteristics. Active

filters can also be implemented without requiring any inductors, which removes the problems related to these components (high cost, widely spaced standard values). In the operating frequency range of the op-amp, the active filter can have very good accuracy [65]. Finally, active filters can be and often are easier to design than passive filters (especially high-order ones) and they also cost less because of cheap op-amps and the absence of expensive inductors.

However, active filters also have disadvantages in that the performance at high frequencies is limited by the active components and the amplifying circuit also generates noise. The noise can be reduced though, by having good and thought-out circuit design [65]. The most commonly used active filters are Sallen-Key and multiple-feedback filters (MFB) (more about these below in Section 3.2.3).

3.2.3 Filter topology

Filter topology defines the filter circuit without the component values. There are both passive and active filter topologies and while the passive filter ladder (also known as Cauer) topology shown in Figure 3.5 is the most commonly used, we will focus more on the active filter topologies. The active filter topologies we are focusing on are the Sallen-Key and MFB topologies, as these are the simplest (least components) and most commonly used.

Sallen-Key topology
The reason why the Sallen-Key topology is often the preferred topology is that the performance of the op-amp has the least effect on the filter performance. This is because the op-amp is configured as an amplifier instead of an integrator. This minimises the GBW requirement of the op-amp and it also means that the GBW does not limit the performance of the filter. This topology is also non-inverting. Furthermore, the gain is independent of the resistors in the filter circuit [66]. The maximum Q factor, however, is rather limited for the Sallen-Key topology, as higher Q factor increases the instability of the filter because of the poles placed closer to the jω axis [67]. The Q factor is also very sensitive to component values [66]. Another drawback for the Sallen-Key filter is that it is not easily tuned because of the component value interactions on resonant frequency and Q factor [66]. Finally, the GBW of the op-amp has to be up to 100 times higher than the cutoff frequency, per (3.1), to not affect the filter response due to the circuit gain being relatively low compared to the minimum required open loop gain of the amplifier [67]. Figure 3.6 shows the Sallen-Key circuit for an LP filter.

MFB topology
Unlike the Sallen-Key topology, MFB filters use the op-amp as an integrator, which means that the transfer function of the filter depends more on the op-amp parameters than it does for Sallen-Key [68]. However, the MFB topology has lower sensitivity to component variations, which is the reason it is often preferred over Sallen-Key. MFB is also inverting if uneven number of stages is used, as the op-amp is used in inverting mode [64]. This could be a problem in some systems or an advantageous feature in others. MFB can also be used to get slightly higher Q factor compared

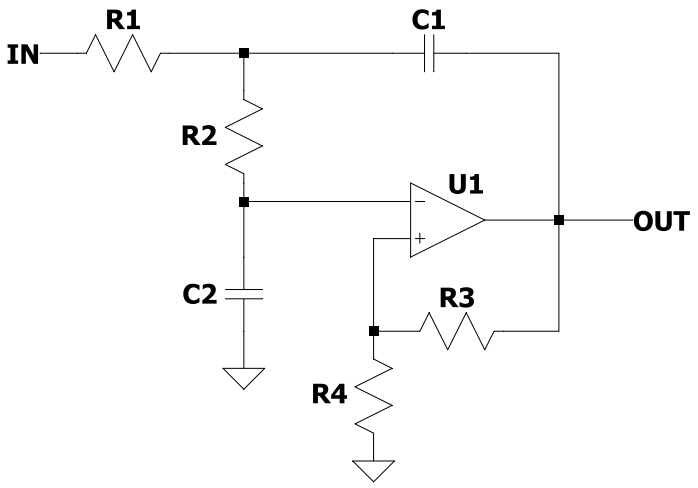

Figure 3.6: Circuit diagram of Sallen-Key topology LP filter.

to Sallen-Key, as the circuit gain is still relatively low compared to the GBW of the op-amp but it is not as slow as the Sallen-Key one [67]. Figure 3.7 shows MFB topology for an LP filter.

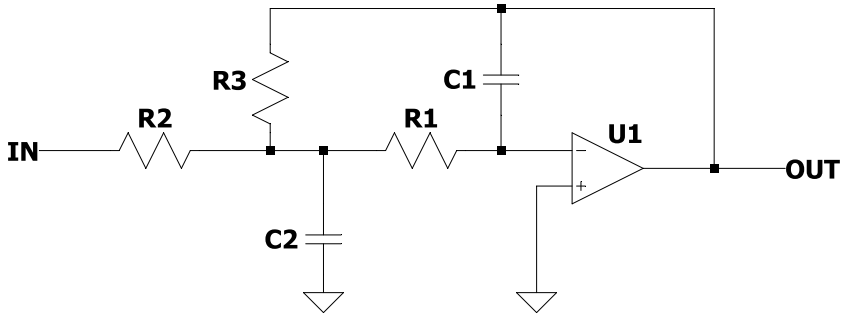

Figure 3.7: Circuit diagram of MFB topology LP filter.

To summarise, Sallen-Key and MFB are similar and both have their advantages and disadvantages. The topology selection greatly depends on the situation. However, Texas Instruments recommends a rule of thumb for situations where Sallen-Key topology is better than MFB: if gain accuracy is important, unity-gain filter is used and Q factor is low [64]. To compare the component count, then for unity gain filter, Sallen-Key has one component less than the MFB filter. However, when there is a need for amplification Sallen-Key requires two additional resistors and then it is the MFB filter which has one component less.

4

System Design

This chapter aims to describe how the system design process was carried out. First section describes the transducer selection process, bringing out the requirements for the transducers and highlighting the transducers we chose from. Next, the filter design is justified, with amplifiers choice closely following, as choosing one of the amplifiers ties back to the filter design. Closing out the components part of the chapter is the additional components section, that describes selection of all the other components, that can be more easily replaced than previously mentioned components.

Then the MCU capabilities are explained and ending the chapter is a section about the mechanical design of plastic tubes which are used as the mounting system for the transducers when testing the sensor system.

4.1 System implementation in hardware

The design of the overall system, as shown in Figure 4.1, was started from the two parts that we knew would be present: the ultrasonic transducers and the MCU. We begun by selecting suitable transducers and tested them to establish suitable inputs and the resulting outputs. Knowing the inputs and outputs we could design the circuit required to transmit a signal generated by the MCU, where we opted for an op-amp based power amplifier to transmit the signal.

Based on the transducer output and the noise picked up by the transducer when in the flow of a ventilator, a filter and amplifier for receiving the signal were designed and a comparator following the amplifier generates a digital timer stop signal at a set point in the received waveform.

To reduce the number of components required we decided to use a multiplexer to change direction of the measurement instead of having one transmitter and one receiver for each direction. The multiplexer's additional channels also doubles as grounding switches for the transducers, preventing crosstalk during transmission from affecting the receiver.

Due to the receiver chain (multiplexer, filter, amplifier and comparator) having a dual-rail signal and therefore dual-supply components, a $\pm 5\,\mathrm{V}$ power supply was also added to the design to convert the $5\,\mathrm{V}$ supplied from the MCU board. The

power block is missing from the block diagram because the later system is expected to be able to supply the necessary voltage levels without the need for a separate power converter.

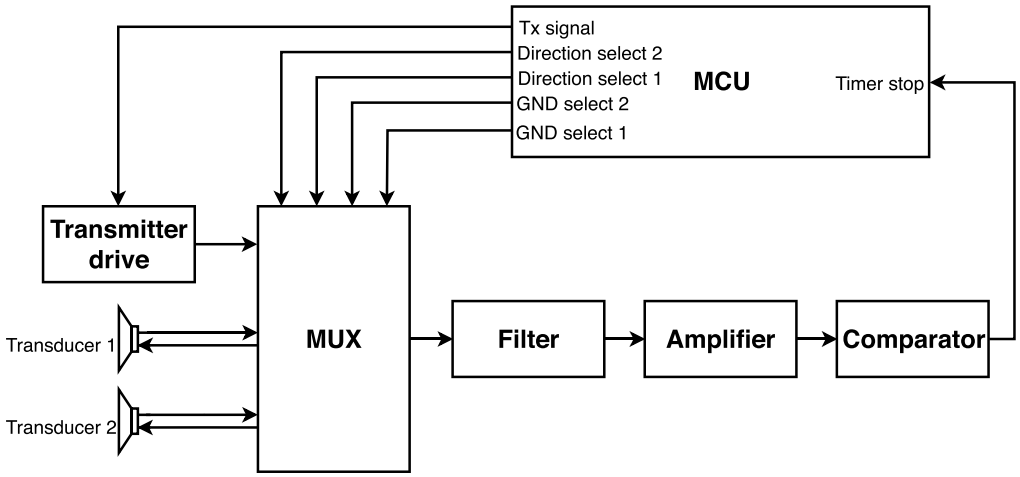

Figure 4.1: Block diagram of the complete sensor system, showing the functional blocks of the design and the signal path from the MCU generating a transmitter pulse to it receiving a time-of-flight stop signal.

4.2 Transducer selection

The transducers were selected based on availability, size, operating frequency, price and transmitted/received signal strength; as we need to send signals in both directions, transceivers, receivers and transmitters were considered. Although there is a research paper mentioning 500 kHz [69] as the most suitable frequency to avoid noise effects while being low enough for attenuation to still be negligible, another gas sensor was found to use 40 kHz [70]; this is also one of the most common operating frequencies for the ultrasonic transducers. Therefore, we decided to start with 40 kHz transducers, as these were the most widely available.

The 40 kHz transducers were also in the acceptable size range for us, as we are trying to fit the sensors into the current system that is carrying out the measurements in a tube that has a diameter of 16 mm. It was one of the main requirements that measuring the gas concentration and flow rate should have a small impact on the gas flow itself and the smaller the sensor, the easier it is to install it in the tube without affecting the flow. Without increasing the tube diameter, the maximum diameter of the transducer was set to 16 mm, although the preferred diameter was set to around 10 mm, so the systems external dimensions would be increased minimally as well.

After researching available transducers on the market, four different models were chosen and tested – two transceivers, one transmitter and one receiver. The transmitter and receiver chosen are a pair recommended to be used together by the

manufacturer. Detailed information about the chosen transducers can be found in Table 4.1.

Table 4.1: Detailed transducer information including dimensions, sensitivity and construction (Min. sound pressure level is at 30 cm and 10 Vrms).

	MCUSD16A40S12RO	MCUSD14A40S09RS	MCUST10P40B07RO	MCUSR10P40B07RO
Type	Transceiver	Transceiver	Transmitter	Receiver
Diameter	16 ± 0.5 mm	14 ± 0.1 mm	9.9 ± 0.3 mm	9.9 ± 0.3 mm
Height (without leads)	12 ± 0.5 mm	9 ± 0.1 mm	7 ± 0.3 mm	7 ± 0.3 mm
Centre frequency	40 ± 1 kHz	40 ± 1 kHz	40.1 ± 1 kHz	38.3 ± 1 kHz
Min. sensitivity	-65 dB/V/ubar	-75dB/V/ubar	-	-70 dB/V/ubar
Min. sound pressure level	110 dB	90 dB	106 dB	106 dB
Operating temperature range	-40 °C to +85 °C	-40 °C to +85 °C	-35 °C to +85 °C	-35 °C to +85 °C
Structure	Open	Closed	Open	Open
Housing material	Aluminium	Aluminium	Plastic	Plastic

As the table shows, there are differences in the signal strength (sound pressure level) and sensitivity. However, it was not fully clear what these differences actually meant for our system. Therefore, we tested the transducers to determine which of these is the best. We tested them in pairs at 3 cm distance. The transducer pairs were made up from two of the same transducer, meaning we had two transceiver pairs, 16 mm and 14 mm, one transmitter pair, 10 mm Tx, and one receiver pair, 10 mm Rx.

The same kind of transducer was used as both transmitter and receiver in each test as the bidirectional measurements of the system means that any performance gained from using specific transmitter and receiver units would be lost when running them in the reverse direction. The same input, a 40 kHz, 5 V peak-to-peak, sine-wave at a single-pulse burst with a 10 ms burst period, was used in all tests to allow direct comparison of the outputs between different pairs. No significant differences in the output waveforms were noticed between square-wave and sine-wave inputs, this led to us instead use square-waves in the later tests as those are easier to create in the final system using a micro-controller. The first pulse amplitude tests were performed with and without a 1 kHz (1.5 nF, 100 kΩ) HP filter to try and get a nicer signal due to the 14 mm transducers' low amplitude.

From the comparison tests we found that the 16 mm transducer was the most sensitive one, with a first pulse amplitude of about 5 mV and second pulse amplitude of about 10 mV, at 3 cm. The 14 mm transducer was the least sensitive one, which was also expected from it being encapsulated in aluminium. The first pulse was hardly discernible from the noise of the measurement, and the sharp increase in amplitude over the first few pulses seen in the other transducers was not observed here, instead not reaching much higher than 3 mV. The two 10 mm transducers, Tx and Rx, were found to perform the same. They both had a first pulse amplitude of almost 5 mV and a second pulse amplitude of about 8 mV. This is less than a millivolt behind the 16 mm transducers first pulse and two millivolts behind for the second pulse.

Considering the test results, we selected the MCUST10P40B07RO transmitter as it is smallest in size and has the 40 kHz centre frequency. The small difference in the signal amplitude between it and the 16 mm transducer does not make up for the 6 mm increase in diameter and 5 mm increase in height of the larger transducer.

We also do not expect the plastic housing to be a problem in the system, so we do not see any clear advantage in the open metal housing design over the open plastic. The closed aluminium housing of the 14 mm transducer does have the advantage of being waterproof, but the much poorer performance makes it an unsuitable starting point when developing the sensor.

4.3 Filter design

To determine what kind of filters and how much filtering the system requires, we first needed to measure the noise present in the system. For this purpose we ran a fast Fourier transform (FFT), shown in Figure 4.2, of the receiving transducer output while it was connected to the output flow port of a running ventilator. We found that most of the higher amplitude noise was in the span below the 40 kHz signal frequency that we are using to measure the time of flight. To prevent system malfunction caused by any higher frequency disturbances, which could be present outside the lab environment, it is still necessary to have a band-pass filter with a LP component, rather than a pure HP filter.

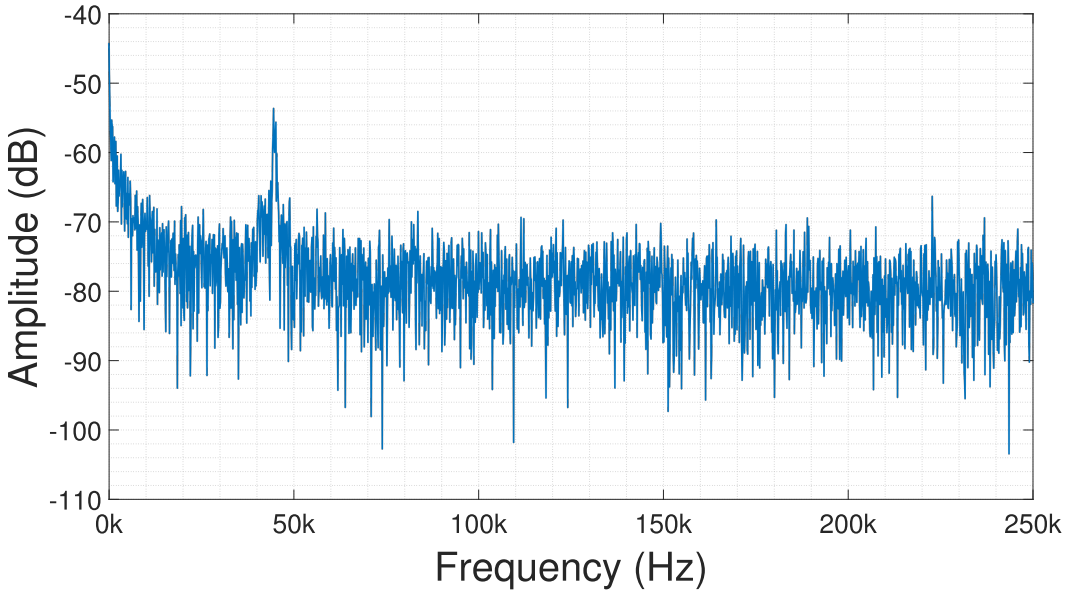

Figure 4.2: FFT of the receiving transducers output when the transducer assembly is connected to the output flow of a running ventilator. The presence of low frequency noise is visible as increasing with lowered frequencies. The peak at 40 kHz is the motor drive frequency, the rest of smaller peaks at high frequencies are also caused by the motor.

However, as we did not discover any high amplitude noise close to 40 kHz, it is not necessary to have a high-order active filter with steep transition bands. Furthermore, we are limited by space and the addition of an active filter on the LP side would have required a higher order filter meaning more op-amps. Therefore, we decided

to use a passive LP filter and an active HP filter to remove the low-frequency noise we saw but still guard against any high-frequency noise as well.

For a passive LP filter the options are RC and RL filters. The RC filter was chosen because capacitors are smaller, cheaper, more widely accessible than inductors present in RL filters. The cutoff frequency for the filter had to be chosen so that it would affect the 40 kHz signal as little as possible. Because a first order RC filter is not very steep, the cutoff frequency had to be placed quite far away from the 40 kHz mark. As a result of simulations in LTSpice [71], where different cutoff frequency values were tested, we decided on 70 kHz as a suitable value. After adjusting the resistor and capacitor values to standard ones, the cutoff frequency of 72.3 kHz was reached.

For the HP filter we had to decide on the frequency response, filter order and topology of the filter. As explained in Section 4.2 mentions, the output frequency of the transducer is not always exactly at 40 kHz, which means that constant group delay is a necessity to be able to compensate for the delay in the calculations. From the three frequency responses introduced in Section 3.2.1, Bessel is the only one with the constant delay which made it our choice of filter.

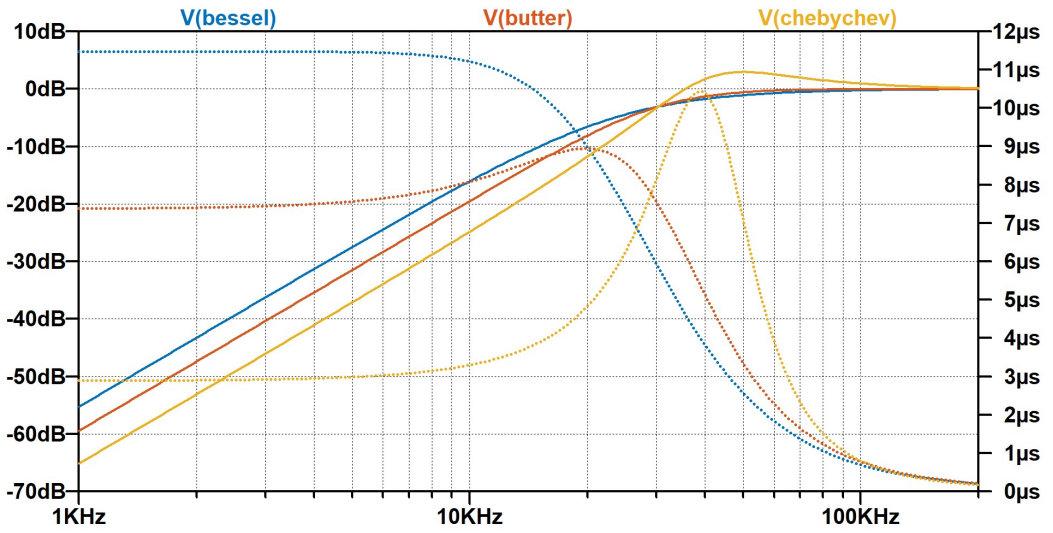

Figure 4.3: Frequency response (solid) and group delay (dotted) comparisons for second order Bessel, Butterworth and Chebyshev HP filters with a cutoff frequency of 30.6 kHz

From Figure 4.2 it can be seen that the noise level under 40 kHz increases around 15 dB per decade. Size restrictions for the board meant that we wanted to keep the filter to as few stages as possible. A second-order filter is the highest filter order possible for one-stage filter, which is the order we started with. As explained in Section 4.2 Butterworth has an attenuation of $20n$ dB/decade (with n being the filter order), making the attenuation for a second-order Butterworth filter 40 dB/decade. We know that our first choice frequency response Bessel has less steep roll-off, while Chebyshev has a steeper one. Figure 4.3 shows frequency responses and group delay of second order Chebyshev, Butterworth and Bessel filters with cutoff frequency at 30.6 kHz, which is far enough from 40 kHz to not affect it much

but still close enough to offer necessary attenuation at lower frequencies. It can be seen, that even though attenuation starts off slow, for the noise level we have second-order filter should still be enough, even when going with our first choice Bessel filter.

Topology choice is once again the one most affected by the size constraints we had for the system and as mentioned in Section 3.2.3 MFB topology has one component less if amplification is needed, which is the case for us. The MFB is also less sensitive to component variations, which is always a good feature. Rule of thumb for choosing Sallen-Key that was mentioned in the same section, mostly does not apply in our case either, as mentioned before, the filter needs to be amplifying but at the same time the gain accuracy is not as important because we are not looking for an exact value after filtering. There was also no problem with MFB being inverting.

The exact values for the active filter components were computed with the help of Analog Devices' Analog Filter Wizard [72] and Texas Instruments' Filter Design Tool [73]. As we had already decided on the filter order, setting the cutoff frequency and filter gain were the only things left to decide. We first set the cutoff frequency to 35 kHz, to leave some space for different output frequencies of transducers and the filter gain to 20 times (26 dB). The resulting values from the tool were adjusted to common values and a filter with 14.67 times passband gain (23.3 dB), 30.6 kHz cutoff frequency and -20.2 dB attenuation at 2.5 kHz was obtained.

The circuit and specific component values are presented in Appendix A.

4.4 Amplifiers

The system has two amplifiers. The first one is a signal amplifier to amplify the received signal from the few-millivolt range up to the 0.25–1 V range suitable for input into the comparator. The other one is a power amplifier, used to amplify the 3.3 V amplitude square wave signal from the micro-controller into a 5 V amplitude signal able to deliver the 60–80 mA required during the signal transients.

4.4.1 Signal amplifier

The output from the transducer at the start of the waveform has an amplitude of about 5 mV. We want to detect when the output of the transducer reaches a specific level and at that point create a digital trigger signal for the MCU to stop its timer. The last step of the amplifier chain is therefore a comparator to perform the amplitude to digital conversion. Theoretically this could be done at the signal level of the transducer output, but two practical problems would arise. First we would need to create a stable reference voltage at a point somewhere around 2.5 to 5 mV and then the overdrive voltage of the comparator is in the same order of magnitude as the 5 mV signal which will slow down the comparison unpredictably [56], [63]. So in practice we want to amplify the transducer output before we use it to create our

digital signal. Higher gain also reduces the time from when the signal passes 0 V to when it reaches the comparators reference level and the lowers impact of amplitude variance on the signal from the transducer.

To both reach suitable overdrive for the comparator, having a range where it is easy to create a reference level for the comparator, and to reach it quickly we want a total gain in the range of 500 to 3000 times. With the active filtering we are using, gain can be incorporated into the filter circuit which allows us to spread the gain and thereby decrease the gain required in any single stage. As described in Section 3.1 pure amplifiers without filters as part of their feedback are limited by the GBW, but filters are often recommended to have much more than that as described by (3.1). This means that we want a second stage of amplification after the filter to reach the required gain without needing large resistance ratios or getting a very high GBW requirement. Therefore, we require an op-amp which is available in a small two-unit package which can be used to implement both the filter stage and the amplifier stage to minimise the physical size required of the circuit.

Opting for using 20 times gain in the filter to calculate the op-amp requirements, (3.1) we get 70 MHz GBW for the 35 kHz cutoff frequency and simulating the circuit in Analog Design's filter wizard gives a lower recommendation of 31 MHz and a bare minimum requirement of 3 MHz. Assuming a lower 10 gain in the filter to dimension the second stage, we need up to 300 times further amplification to hit the upper bound of 3000 times amplification, which at our signal frequency of 40 kHz gives a GBW requirement of 12 MHz, much less than any recommendation for the filter. So the filter is the limiting part in selecting an op-amp with sufficient GBW of at least 30 MHz.

The filter design further limits the op-amp selection by the high-pass characteristic removing any DC component, which would need to be reapplied to use a single-supply amplifier. Rather than reapplying the DC component through a more complex signal path circuit, it was decided to use a dual-supply chip powered by a slightly more complex power supply circuit.

The input bias current of the op-amp, as desribed in Section 3.1.2, is another important factor in selecting the correct chip. As an example a 1 µA input bias would across the filter create a 5.1 mV offset, which then would be amplified by the amplifier stage for a total of 127 mV offset. Such a large offset would not be acceptable with a 2 V range output, so a low, nanoampere range, bias current is required. The input offset voltage is of less concern as the high input impedance of the op-amp along with the high-pass characteristic of the active filter keeps the amplification of the offset low.

From our requirements of a small package, two-unit dual-supply op-amp with at least 30 MHz GBW, low input bias current, we found the AD8034 [58]. It is a dual-supply op-amp of 80 MHz GBW with a typical input bias current of 1 pA available as two units in the 8 mm^2 SOT-23 8-pin package.

4.4.2 Power amplifier

A transmitter signal that can supply some current is required to power the transmitting transducer. When testing the transducers we found that powering the transmitter by a 40 kHz squarewave gave a receiver output no worse than when powered by a sinewave. The lack of a difference between using sine and square input allows us to use a simple transmitter amplifier with only two output values that can easily be generated by a pulse-width modulation (PWM) signal from the MCU.

The transducer was tested in series with a 10 Ω resistor, powered by a function generator supplying a 40 kHz, 5 Vpp, squarewave at a single-pulse burst with a 10 ms period to establish the current through the transducer. This experiment showed that the transducer only consumes power during the transients of the square wave, quickly returning to zero after 100 −300 ns from the start of the transient. The average current during these short periods was at most 80 mA and on average about 60 mA.

The transducer could be powered directly by the PWM output of the MCU, but this solution would both limit the operating voltage of the transmitter to no more than 3.3 V and be, even if momentarily, a quite large load for the MCU inputs/outputs (I/O) that are not designed to supply currents above 20 mA [74].

Three alternatives were considered to create the power amplifier: the use of a transistor together with a pull-up (or down) resistor [57], the use of an inverter as shown by [75] and [46], or the use of an op-amp as a low-gain amplifier. Due to the simplicity and size of the circuit together with the lowest count of passive components required, we first examined the second alternative, that is using an inverter for the transmitter amplifier.

Our requirements when selecting the inverter were a small footprint, high continuous current rating, 5 V operation and the ability to function correctly with a 3.3 V input when supplied by 5 V. We found that most inverters have around 70% of the supply voltage as their logic input high voltage level. With a 5 V supply this level is 3.5 V, which is above the logic high voltage output level of our MCU. We found one inverter, the ON Semiconductor MC74VHC1GT04 [76], which in its datasheet states that it is suitable to operate with a 3.3 V input when supplied by 5 V. The specification tables in the datasheet are however inconclusive in how well it performs then, with only the minimum voltages for the logic level high listed while the maximum acceptable voltages for where it starts are not published. When testing this inverter we found it to require about 3.5 V to detect a high input level, making it unusable for our purpose. The use of an inverter as the transmitter amplifier was therefore not further considered as an alternative.

With a transistor or an op-amp solution as the two remaining alternatives, they were compared to each other. They require a similar number of passive components: two feedback resistors to set the gain of the op-amp or a pull-up (or down) resistor to counteract the transistor. But as described in Section 3.1.1, the counteracting resistor on the transistor will act as an additional load, limiting the delivered power or increasing the power consumption. The op-amp does not have this skewed supply

limitation, which made it the solution of choice over the transistor.

Multiple op-amps capable of supplying a current of at least 100 mA at a frequency of 40 kHz were found. As the op-amp is generating a 0 to 5 V square wave and the peak power exceeds the limits of the +-5 V power supply, a single-supply op-amp was therefore required so that it could be powered from the board supply rather than from the double-supply DC/DC converter. Three suitable op-amps were found: the AD8591 with a 5 V/µs slew rate and 250 mA output rating, the AD8615 with a 12 V/µs slew rate and 150 mA output rating and finally the ADG4891 with a 170 V/µs slew rate and 125 mA output rating. The current rating for all three devices is more than adequate and so is the slew rate for a 40 kHz sine, which requires

$$f\, 2\pi\, Amplitude\, 10^{-6} = x \text{ (V/µs)} \tag{4.1}$$

or 1.2 V/µs for 40 kHz at 5 V. But as the system uses a square wave a higher slew rate is preferable and having it higher also makes it possible to test the circuit with a transducer operating at a higher frequency in the future, without replacing active components. Hence the ADA4891 was selected as the transmitter driver.

To generate a 5 V amplitude square-wave out of the MCU supplied 3.3 V amplitude square-wave the op-amp is connected in a non-inverting configuration with a gain of 2. This way the 3.3 V high signal is easily amplified to the max-rail of 5 V while removing any risk of a "not-quite zero volts" low signal being amplified by any significant amount. The input offset voltage is also small enough, at a few mV, to not matter when driving a transducer.

4.5 Additional components

This section describes the design process behind selecting the rest of the components – multiplexer, comparator, power supply, capacitors and resistors. These are the components that were chosen to fit in with the other components, as they perform simpler tasks and are not as crucial (meaning that they can more easily be replaced by other similar components) to the system as the components mentioned in previous sections.

4.5.1 Multiplexer

There were three main requirements for the multiplexer. Firstly it had to a have low signal resistance, so it would not affect the filters and there would not be a voltage drop in the tx signal. Secondly, we wanted high separation between the outputs, so that they would not affect each other. Thirdly, the digital input logic high had to be low enough that the multiplexer would work with a 3.3 V control signal from the MCU. A small package and operation from 5 V supply voltages were also preferred attributes.

We needed a bidirectional multiplexer/switch that could switch between two inputs for two separate outputs, two single-pole double-throw (SPDT) switches, to change

which transducer is receiving and which is transmitting the signal. We found three suitable chips that all had two independently selectable switches – ADG844 from Analog Devices and TS5A23160 and TS5A23159 from Texas Instruments. All multiplexers had low resistance of 1 Ω or below and the channel-to-channel crosstalk values were also almost on the same level for all (-60 dB for AD multiplexer and -64 dB for TI ones). However, ADG844 had an input logic high of 2 V, while the others had it at 2.4 V. This feature together with it having a working spice model, made ADG844 the preferable multiplexer for our system.

After testing the ADG844 it was found that the crosstalk between channels was too high, which resulted in that the receiving transducer also begun to ring from the transmitting transducer's input signal. The ringing persisted long enough to interfere with the arrival of the soundwave at the receiver which leads to inaccurate time-of-flight measurements. In the worst-case scenario this interference is completely out of phase with the arriving wave which then would make it impossible to tell when the wave arrived as it would first have to dampen the existing ringing. To solve this problem we decided to add the ability to ground both terminals of the receiver during transmission, as the time of flight separates sending the transmission from receiving it and there is ample time to release the signal terminal from ground before the soundwave arrives. This modification meant that two additional channels were required to be able to ground both transducers, separately.

This could either be achieved through adding a separate chip with more multiplexers or switches, or it could be achieved through using another chip containing additional channels. The latter alternative seemed more efficient so the search for a suitable multiplexer was extended to chips containing four separately controllable SPDT circuits along with the previous requirements. We found that all four channel chips from Texas Instruments that fulfilled the other requirements lacked the separated channel controls but from Analog Devices a suitable chip was found: the ADG1634 which has four channels and a slightly higher, but still low, resistance of 4.5 Ω along with a better than the ADG884 channel-to-channel crosstalk at -64 dB and an input logic high of 2 V.

4.5.2 Comparator

The main requirement for the comparator was that it had to work with an input signal spanning both positive and negative values, as the signal coming from transducers swings around zero, and we did not want to bias the whole system to get rid of the negative part of the signal. Another necessary requirement was for the comparator to have an output signal that swings from ground to positive rail, rather than rail to rail. This output range allows the output signal of the comparator to be sent to the MCU digital input pin for the time-of-flight measurement with minimal processing. The supply voltage (preferably working with 5 V), delay, rise time, overdrive and small package size were also important points when choosing the comparator.

As it was important for us to be able to simulate how the system acts, we first went through the components available in LTspice and found three different comparators

suitable for our system – LT1711, LT1016 and LT1713. LT1711 had the lowest delay (4.5 ns) and also the fastest rise time (2 ns) making it the best option from the Analog Devices catalogue. We also surveyed Texas Instruments and Maxim Integrated products but we did not find any comparator that had better characteristics, therefore LT1711 is our comparator of choice.

4.5.3 Power supply

The main power to the sensor is supplied by the existing MCU system at 3 V, 5 V and 24 V. But as it was decided to use dual-supply components rather than adding a DC bias to the transducer and the op-amp signals to get a single-ended signal, an additional power supply of -5 V is required. Instead of designing a power supply ourselves, which was considered outside of the scope of the project, we opted for an integrated solution in the Murata MEA1D0505SC 5 V to ±5 V, 100 mA, DC/DC converter which will be used to power the dual-supply components.

4.5.4 Passive components

Together with the active components, there are also a number of passive components used throughout the design. All resistances were selected from the E24 range at 1% tolerance and for the prototype board of the 0603 size [77]. Smaller resistors could be used in many places throughout the design, but would make any manual soldering very difficult.

Capacitors appear with two different purposes in the design. In the filtering for the receiver amplifier, 5% tolerance film capacitors were used to ensure accurate capacitances over temperature and charge variation. These capacitors are not available in sizes smaller than 0805 [78], so those were used. Meanwhile for decoupling of the active components, where the exact capacitance is of less importance, ceramic X5R capacitors in the 0603 size were used throughout the design.

Only a single pair of inductors appear in the design as part of the recommended output filtering of the DC/DC converter. For this filter we used the 1210 [79] sized inductors recommended for the purpose by Murata [80].

The worst-case impact of the passive components tolerances was simulated in LTSpice by simulating all combinations of maximum and minimum values allowed by the tolerances. We found that the largest amplification increase at 40 kHz was 0.8 dB, or about 10%, and the largest decrease was 0.5 dB, or about 6%. This variance is acceptable since we are not detecting the absolute peak of the waveform but the rising edge, so any constant change in amplification will appear as small time-constant offset from the detection point being reached slightly earlier or later and should be possible to compensate.

4.6 The MCU

The capabilities of the STM32F765IGT6 MCU were evaluated to establish if it would impose any considerable limitations on the performance or function of the sensor. As the core measurement of the sensor is time-of-flight, the timers were the first part to be evaluated. The timers in the MCU are capable of running at speeds up to the maximum system clock of 216 MHz [81]. To get an idea of what impact different clock speeds would have on the TOF measurement, Table 4.2 was created to show the magnitude of the error caused when the timer stop signal arrives at the maximum delay possible from the timers counter increasing, leading to a measurement error equal to one clock cycle.

Table 4.2: The effects of timer error at four frequencies up to the maximum timer frequency of the MCU. The reference speed of sound, c, was set to 386.47 m/s to correspond to a case where some flow is present or the temperature is higher than ambient and the distance was set to 4 cm.

Timer frequency (time offset)	Measured TOF (m/s)	Absolute error to TOF (m/s)	Error relative c (%)	Oxygen concentration error (%)
1 MHz (1 µs)	390.24	-3.77	0.98	-17
10 MHz (100 ns)	386.85	-0.37	0.097	-1.7
100MHz (10 ns)	386.51	-0.037	0.0097	-0.17
200MHz (5 ns)	386.49	-0.019	0.0048	-0.084

The table shows how the lower timer frequencies of 1 MHz and 10 MHz have a large impact on the accuracy of the oxygen concentration, where 1 MHz has an error of up to 17 % and 10 MHz has the more reasonable but still high error of up to 1.7 %. The errors are however reasonable for the 100 MHz and 200 MHz estimates, at 0.17% and 0.084% and we consider the timer to be fast enough for our measurements.

The second step in evaluating the timer was evaluating the counter registers required when running a timer at 200 MHz by calculating how quickly the counter can count to the end of the register. For a 16-bit register this takes approximately 325 µs, which corresponds to a distance of 11 cm at ambient speed of sound, which is further lowered by opposing gas flow and lower temperatures increasing the TOF. Hence the 16-bit registers were deemed too small for our measurement, but the MCU also has two timers with 32-bit registers, which meant that using one of those timers became a requirement to use the MCU.

In addition to the timer that measures the TOF, timers are required to create the transmitter signal and the two signals used to ground the currently receiving transducer during transmission, through PWM output. But these timers do not need to run for more than 300 µs, and three 16-bit timers are available that can be started together with the 32-bit timer used to measure TOF [81]. Each of these timers can support up to 4 PWMs, so these three signals can be generated with as little as a single additional timer.

Finally an output is required to control the direction of the transmission, but as this takes place between measurements there are unlike the other signals no strict timing requirements and can be controlled by general purpose outputs, which are

readily available. The signals required between the MCU and the sensor are shown in the timing diagram of Figure 4.4 which covers a complete measurement of two samples, one in each direction (0-25, 50-75) including the two ground windows (Gnd 1, 2), the direction select (Dir), the transmitted signal (Tx) and the received signal (Rx) from the comparator. The TOF is marked for both directions, the time scale is selected to help show the communication conceptually and is therefore not real.

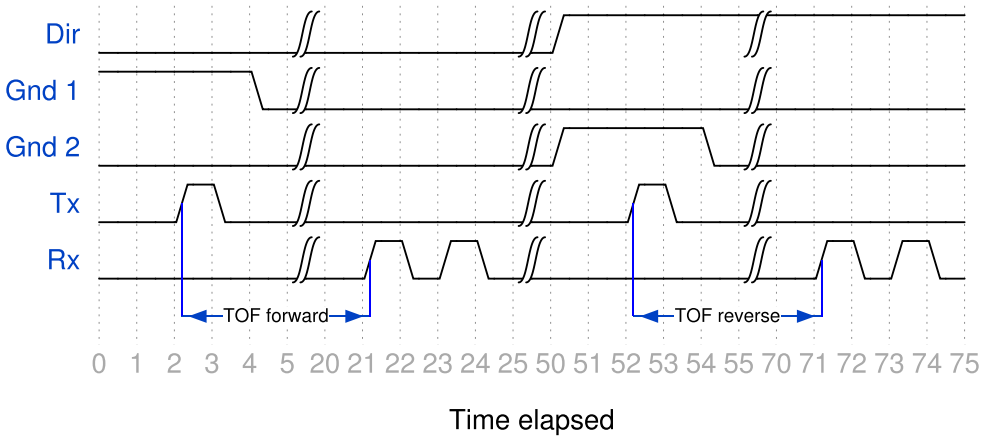

Figure 4.4: Timing diagram of the signals between the MCU and the sensor. The diagram covers a complete measurement of one sample in each direction at times 0-25 and 50-75, with the direction select signal Dir, the ground windows Gnd 1 and 2 for respective direction, the transmitted signal Tx and the sensors comparator output of the received signal Rx. The time scale is chosen to illustrate the communication and is therefore not real.

As the MCU is a fairly powerful device, running at 216 MHz, we foresee no issue in performing the calculations required to convert our measurements into concentration and flow values in real time.

4.7 Mechanical test structure

To facilitate testing of the system, a mechanical structure where the transducers can be mounted across a flow path is required. The flow path was set to have 15 mm inner diameter, to match the standard sizes of the ventilator. The other primary attribute of the structure is the angle of which the transducers' path intersects the flow. For liquids, simulations have shown that the optimal angle to limit the impact of turbulence in the flow is 75 degrees to the flow axis [82], but this steep an angle gives a very short distance between the transducers and a very small flow component, possibly limiting accuracy. A similar issue appears with using shallow angles, where the minimum distance between the transducers becomes very long. It was decided to have three structures manufactured with different angles, 35°, 55° and 75° to allow testing of the impact of the angle within the span where it was deemed neither too steep nor too shallow. The structure we required was first drawn by hand to establish the required measurements and then transferred to 3D

cad with the help of a mechanical engineer at i3tex and sent to be manufactured by a mechanical workshop. The drawing can be seen in Figure 4.5.

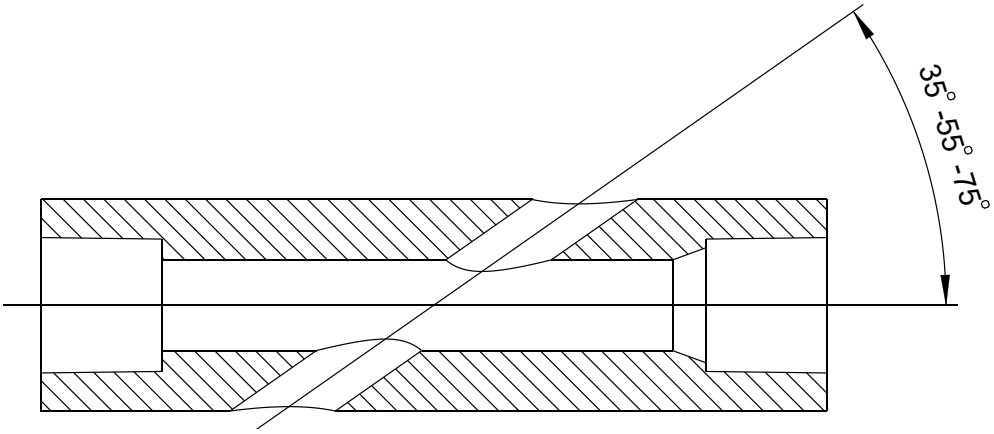

Figure 4.5: Drawing of the mechanical test structure with the 15 mm horizontal flow path through the sensor and the 10 mm angled transducer path. Both ends of the flow path have adapter cones for tubing and one side has beveled edges to minimise the disruption of the flow. Right to left makes the forward flow direction and left to right the reverse flow direction. Drawing by Lars Bolander, i3tex AB.

4.8 Alternative hardware solutions

There exists at least one application-specific integrated circuit solution on the market with the intended purpose to perform the same kind of ultrasonic flow and concentration measurements as our sensor. This is the Texas Instruments TDC1000 Ultrasonic Analog Frontend [83] and the TDC7200 Time-to-Digital Converter [84]. Here, the TDC1000 takes the role of our sensor board, containing amplifiers, multiplexers and comparators to generate timer start and stop signals when started by an MCU through an SPI interface. The TDC7200 takes the role of the timers in our MCU, starting to count when it receives the start signal of the TDC1000 and counting the duration untill up to five stop pulses which it then delivers to the MCU through an SPI serial interface. The main differences between this solution and our design are the larger number of features integrated into single chips, the use of serial interfaces rather than having the MCU control the analog components and run the timers, a higher resolution timer which does require an external clock and the limitation of saving the duration of only five TOF values.

5

Design Implementation and Test Results

This chapter gives an overview of the resulting hardware and software of the system. The PCB design, software solution and mechanical build will be described and testing and verification results will also be introduced.

5.1 PCB schematic and layout design

The schematic and layout design were both done with some important considerations in mind. Firstly, from the requirements (Section 1.4) came the size limitation, with the goal being that the board should be as small as possible while still maintaining its functionality. Another thing that had to be considered was as we wanted to be able to hand solder the board ourselves, the components had to be large enough and the integrated circuits (ICs) could not have pins under them. The board had to also be easily testable, which meant that multiple test points were needed. Finally, the layout had to also be designed so there would be as little noise as possible while still fulfilling the previous requirements.

The schematic of the system is directly based on the components chosen in Chapter 4. All the additional components were added to improve noise performance or protect the circuit and their functions are discussed below. The schematic itself can be found in Appendix A. The 3D model of the PCB is shown in Figure 5.1 and all the components mentioned below can be found both in the schematic in Appendix A and in Figure 5.1.

The designed PCB consists of two layers, i.e., the signal layer and the ground layer, and its size is 56 $\times$ 37.5 mm. The board has 12 I/Os that are divided between two connectors J1 and J2 (blue components in Figure 5.1). J1 connects the board with the MCU and has six input pins, one output pin and a ground pin, while J2 connects the board with the transducers. J2 has two transducer I/O pins and two ground pins between them to ensure the isolation between the two transducer channels. Transient-voltage-suppression TVS diodes placed close to connectors were chosen to protect the board from being damaged by electrostatic discharge (ESD) as they quickly clamp transient voltages to safe levels. As transducer outputs can have both positive and negative voltage levels bidirectional TVS diodes (D1 an

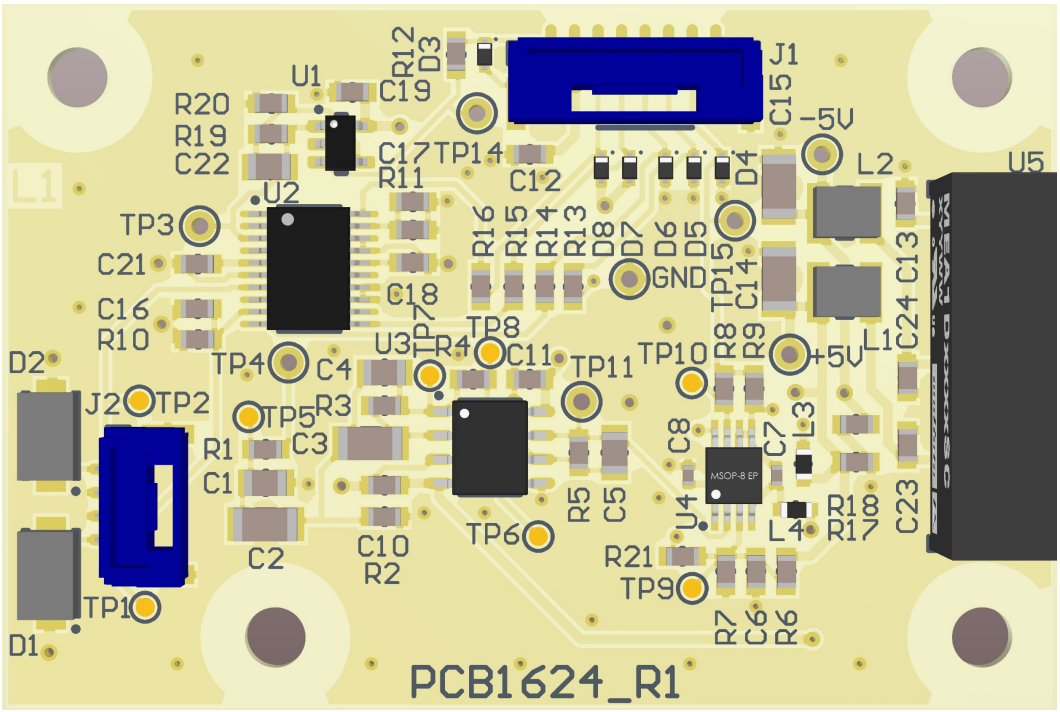

Figure 5.1: PCB layout of the final board

D2 in Figure 5.1) are used for transducer connections and unidirectional (D3 - D4 in Figure 5.1) for only positive voltage level MCU connections. The transducer connections have also input protection to prevent any voltage build up which the transducers can accumulate from mechanical and thermal changes while they are in a floating state [85].

The board is mostly analog, the digital signals are only used to generate the signal for transmitting transducer, control the multiplexer and send a timer stop signal back to MCU. The digital signals are all on the upper side of the board.

The board has four chips – U1 is the transmitter power amplifier (ADA4891), U2 is the multiplexer (ADG1634), U3 is the dual-package signal amplifier (AD8034) and U4 is the comparator (LT1711).

The gain of transmitter amplifier is set at two by the two resistors R19 and R20 and there is a possibility for a LP filter by adding a capacitor C22 if necessary. The band-pass filter is made of passive LP and active HP filters as mentioned earlier in Section 4.4.1, the HP filter uses one op-amp from the dual-package U3. The other amplifier is used for final signal amplification before comparator. HP filter gain is set by capacitors C2 and C4 and the amplifier gain by R5 and R4 and there is a possibility of adding LP filtering to this amplifier stage with using capacitor C5.

The comparator we are using is a high-frequency one and therefore needs additional attention; the layout was done so the input and output pins would be isolated from one another. In addition to that we also use smaller decoupling capacitors here than

everywhere else to improve the performance at higher frequencies. In series with the supply inputs we also added ferrite beads to further suppress any high-frequency noise. For setting the reference voltage a voltage divider was used. Another voltage divider is also on the output of the comparator to lower the comparator high level output voltage of 5 V to 3.3 V to be suitable for interfacing with the MCU.

U5 is the DC-DC power converter for converting 5 V into +5 V and -5 V required because the comparator and power amplifier are dual-supply components needing both positive and negative voltages. The power converter circuit consists of load resistors that are needed to supply the correct level output voltages and HP filter to suppress the ripple otherwise affecting the DC output signal.

In addition to all the previously mentioned parts of the system, there are several additional decoupling capacitors and both through-hole and surface-mount test points. Through-hole test points were chosen for the places in the circuit that need more monitoring during verification, testing and debugging. The board also has four screw holes suitable for M3 screws for mounting the board into the system.

5.2 Creating the software

We began the software development by evaluating which peripherals were available on our development board through pin header connections, rather than hardwired to specific functions. Due to the requirements of both using a 32-bit timer for the time of flight measurements and the ability to perform a synchronised start of all the timers, only one viable peripheral configuration was identified which had a pin configuration suitable for the development board and this was therefore implemented.

This configuration uses the 32-bit TIM5 timer to measure the TOF, where channel 2 is configured to save the time of each rising edge and channel 3 the time of each falling edge. Direct memory access (DMA) is used to save the times of rising and falling edges for all pulses generated during a measurement without requiring an interrupt to trigger for each edge of each pulse. TIM3 timer channels 1 and 2 are set in single shot PWM mode to generate the ground window signals when enabled. the TIM4 timer channel 1 is also set in single shot PWM mode but to generate the transmitter pulse at the end of the ground window and it is set to operate in master mode, the other two timers are slaved to this timer which makes them all start together when TIM4 is started. The measurement direction switching is not timing critical and is therefore performed during the interrupt at the end of a measurement. Two general purpose outputs are configured as outputs for this purpose. This configuration covers the signal requirements of the sensor shown in the Figure 4.4 timing diagram while expanding the Rx channel to also save the falling edge timings to calculate the peak of the Rx pulse.

We configured the peripherals through STM32CubeMX, a peripheral configuration software for the MCU from its manufacturer STMicroelectronics. This tool generates initialisation functions in C from a graphical user interface which reduces the time spent mapping the wanted configuration to the control registers of the peripherals

to almost nothing, leaving only slight tweaking and verification. These C functions were used as the starting point in initialising our software, with manual edits to tweak the configuration as the development progressed.

After adding the peripheral configurations to the program, the peripherals were enabled one at a time to verify their respective function. After having verified all the peripherals separately through the use of live debugging and a logic analyser, the timers were chained together through the master-slave functionality and the DMA of the TOF timer was enabled so that they all could be verified to work together. The program was then extended to handle the resulting data and restart the timers at the "end of timer" interrupt of the TOF timer. This way consecutive measurements are made by only starting the first measurement externally and then the interrupt continues by starting the next measurement until the measurement series is complete or, in the case of continuous monitoring, forever.

The development board is designed to use a UART serial interface for communication with a computer and we enabled this also in our software. We parse the received data in our main loop as an interface to control the sensor and we send the results back at the end of the interrupt of each complete measurement (every second interrupt) after starting the next measurement cycle as to not impose any additional delay between measurements. The commands were implemented with a $KeyValue$ format where the letter signifies what the command is and the number the value to set, if applicable, e.g. $t22300$ to set the temperature to 22.3 °C or r to start the sensor. The full list of commands implemented is available in Table 5.1. The units are not necessarily their base SI unit but instead scaled to fit sufficient accuracy into an integer, without requiring a decimal point.

Table 5.1: Table of the implemented control commands, all values ranges are limited to 32 bit signed integers unless otherwise noted.

Command	Key	Value	Description
Run	r	None	Starts or resumes a measurement series.
Stop	s	None	Stops the current measurement series.
Pause	p	None	Pauses the current measurement series.
Identifier	i	Identifier number	The numerical ID for the measurement series.
Temperature	t	Temperature in mC	The temperature in the sensor.
Distance	d	Distance in µm	The distance between the transducers.
Angle	a	Angle in degrees	The angular offset of the transducers to the flow.
Pressure	e	Pressure in Pa	The pressure in the sensor.
Absolute offset	o	Offset in clock ticks	The offset in clock cycles that is subtracted from a sample to compensate for constant delays.
Differential offset	u	Offset in clock ticks	The differential offset between the two directional measurements to compensate for any difference.
Number of cycles	n	Number of cycles	The number of measurements to run.
Humidity	h	Humidity in percent	The current humidity of the air.
Flow scaling	k	Scale factor × 1000	The scale factor for the flow measurement. Set value is divided by 1000 when it is used.
Filter window	f	window length (1-32)	Sample length of the moving average filter.

After implementing the serial communication, we implemented the equations required to calculate flow and oxygen concentration from two consecutive samples

along with the environmental parameters configurable through the control commands.

5.3 Implementing the equations

The TOF timer records many pulses from the sensor board in each measurement. From the TOF of a pulse in known conditions, together with the offset and distance, it is possible to calculate the range where this pulse will appear under other conditions through (2.1) and (2.6). This is done by taking the fastest, 360 m/s, and slowest, 320 m/s, possible speed of sound for our temperature and oxygen concentration range. Then flow corresponding to about 18 m/s, or 420 l/min at 35° with a flow scaling of 2.2 (our least flow capable angle) is added or subtracted to these values to get the two extreme points. This gives a range in time which is slightly less than one period of the 40 kHz ultrasonic signal, which ensures that only one, specific, pulse will appear within the range. By selecting the rising edge sample of the measurement within this range together with the first falling edge sample after the rising edge, the same pulse is selected each time. The flow range can be extended by including the current temperature in the equation, lowering the possible span of the speed of sound to only depend on the concentration change, which is at most 27 m/s per (2.6). Then the maximum flow can be increased by around 13 m/s up to approximately 31 m/s or at least 725 l/min. But as the sensor only has a manually updated temperature value and 420 l/min is more than the ventilator used for flow and concentration testing can supply, this functionality was not implemented in the software. If the angle of the transducers is increased, so is the maximum flow capacity per (2.12), but this also amplifies any error in the TOF measurement.

To increase reliability and to give the receiving transducer time to get in phase with the incoming wave, the window was configured to select the 4th valid pulse in air at room temperature rather than the first one. Letting it move into phase gives a more stable measurement which reduces the time variance and the additional energy from the incoming sound wave increases the output amplitude of the transducer. This is important when measuring higher oxygen concentrations as we observed an attenuation effect of up to 40% of the normal output amplitude at 100% oxygen. When trying to detect the much weaker first pulse, this attenuation was large enough to push the amplitude of the first pulse below the comparator threshold.

Having selected the specific pulse to use in the calculations, the time of flight for the rising and the falling edges of the timer signal are added together, the offsets are subtracted and the moving average filter is applied by replacing the oldest saved value with the new one and calculating the new average. Every second measurement, after the TOF of both directions has been recorded, the average and the differential velocities of the two samples are calculated.

The differential velocity, which is the flow through the sensor in meters per second, is calculated according to (2.12) using the set distance, angle, the timer clock speed and also the flow compensation factor. The flow velocity is then converted to

the STPH compensated litre/min value through (2.13) using $a = 1.767 \times 10^{-4}\,\mathrm{m}^2$, corresponding to the 15 mm sensor tube diameter, and (2.14) is used to relate the current pressure and temperature to the reference conditions.

The average velocity, which is the speed of sound in the sensor in meters per second, is calculated from the average TOF of the two directions of measurement and the distance between the sensors according to (2.1). The speed of sound is then used to calculate the concentration of oxygen in the air using (2.11) along with the temperature. The remaining variables in the equation, which depend on the pressure, temperature and humidity of the air, are calculated and updated only when any of those variables changes values.

5.4 System calibration

The control commands of the system cover two kinds of environmental variables. First there are those which are environmental properties such as temperature and humidity that have to be supplied for the calculations and can change during operation. Second there are those which are sensor properties such as transducer distance and timer offsets which need to be calibrated for the sensor to function properly in its current configuration.

There are four variables which fall into the calibration category, the absolute offset, the differential offset, the sensor distance and the flow compensation factor. The flow compensation factor is a simple scaling of the flow measurement to compensate for the geometrical factor in the flow equation (2.12). The differential offset, similarly, is used to tune the flow to zero, at zero, which compensates for any offset between the two directions of measurement when there is no flow through the sensor.

The two remaining variables, absolute offset and sensor distance, are used to calibrate the oxygen concentration measurement through (2.1). The distance, d, controls the slope between the two end points of the measurement range and the offset, subtracted from t, controls the offset from zero. The expected speed of sound at the 20.9% oxygen concentration of air (c_{20}) and at 100% (c_{100}) can be calculated using (2.6) and by running the sensor in 20.9% and 100% oxygen the TOF for these two points (t_{20}, t_{100}) are measured. Combining the speed of sound equations (2.1) for both oxygen concentrations we can solve first for the offset

$$\text{offset} = \frac{t_{20} \times c_{20} - t_{100} \times c_{20}}{c_{20} - c_{100}} \tag{5.1}$$

and then the distance

$$d = c_{20} \times (t_{20} - \text{offset}). \tag{5.2}$$

This way both endpoints of the measurement span are calibrated to their expected positions and it does mean that the distance is no longer directly tied to the physical distance between the transducers but rather adjusted to also include any other linear delays of the system. Measuring the distance was the first method tried and resulted in measurements reaching upwards of 125% oxygen concentration with the offset

calibrated for 20.9%, a large obstacle in physically measuring the distance is finding the exact internal position of an encapsulated transducer.

5.5 Setting the sample duration

The first test was establishing the fastest sample duration which our sensor could successfully be run at. The sensor was run at the ambient conditions with no flow or additional oxygen and a measurement series was performed where a thousand measurements were taken for each sample duration at 1 ms intervals from 1 ms to 7 ms. In Figure 5.2 the plot of the resulting TOFs in timer ticks are shown in order of increasing sample duration for each series of 1000 samples. The forward direction uses the thinner line and the reverse direction uses the thicker line.

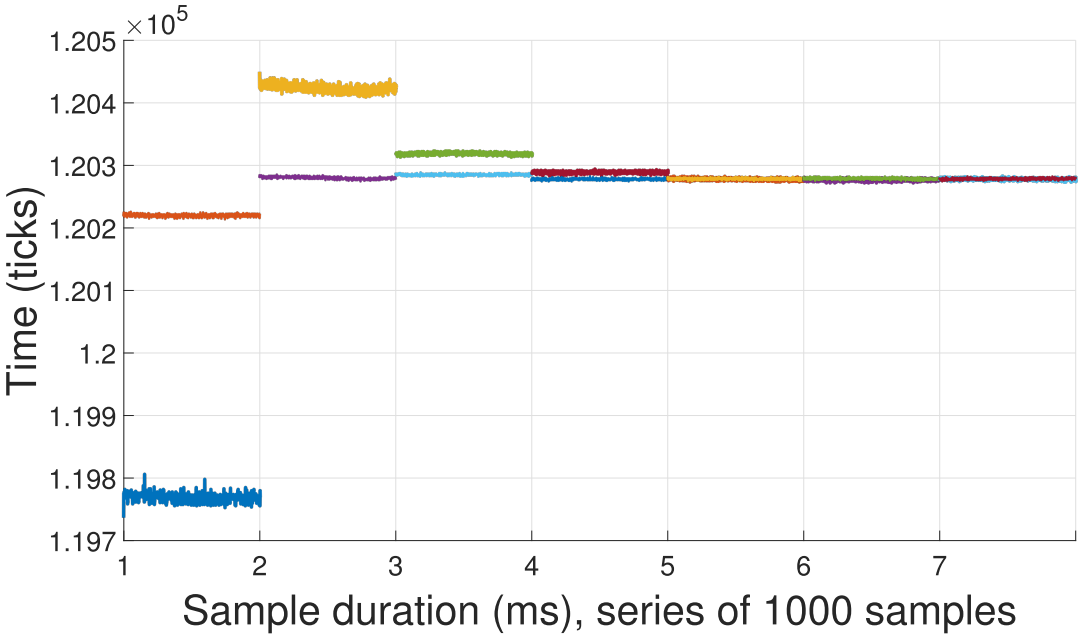

Figure 5.2: Figure of the TOF in ticks for both directions of a measurement without flow (thin forward, thick reverse) for 1000 samples at seven different discrete sample durations. The expected result is that there is little to no difference between the two directions. When the duration is too short, the transducers are still ringing as the direction is switched which will causes incorrect measurements.

As the measurements were taken with no flow, the expected result of a viable sample duration is that the TOF in both directions is close to the same and that they converge to a value that is the same across durations as the duration increases. This occurs first at the 5 ms sample series and this is also the point when it converges with longer durations. At the shorter durations it can clearly be seen how the forward direction (thick) deviates quicker from the expected value than the reverse direction (thin). This was found to be caused by the receiving transducer in the forward direction ringing for a longer duration from acting as a transmitter in the previous

sample, than the other transducer had after the change to the reverse direction. If this happens due to variation in the transducers or in the multiplexer has not been established, but it means that the minimum duration of a sample is at least 5 ms, requiring about 10 ms per measurement, a sample rate of 100 Hz.

After establishing that the system was stable in no flow from 5 ms, it was tested with flow and oxygen. The flow was set to a constant 30 l/min and the additional oxygen part of the flow was varied from 0 to 6 l/min of the 30. During these tests it was found that the change in oxygen concentration also affected the flow measurement. The largest variance was seen at the 5 ms sample duration, with a constant deviation of as much as 5 l/min depending on the amount of oxygen added. At 6 ms the maximum deviation decreased to about 1.5 l/min and at 7 ms it was less than 1 l/min. Hence, the sample duration was increased to 7 ms, leading to a measurement duration of about 14 ms or a frequency of 70 Hz.

5.6 Evaluating the sensor performance and capabilities

With the sensor designed then calibrated for linear factors and offsets, the performance and sensing capabilities of the sensor were tested with both oxygen concentration and flow. We used the Citrex H4 and the IMT FlowAnalyser, two flow analysers with oxygen concentration sensing capability as reference sensors in our measurements. The Citrex H4 is capable of measuring flows of up to 300 l/min with an accuracy of 1.9% of the reading and an absolute error of 0.1 l/min, temperature from 0 to 50 °C at 1.75% of the reading and an absolute error of 0.5 °C and it can measure oxygen concentration with an accuracy of 1% [86]. The FlowAnalyser is also capable of measuring flows of up to 300 l/min but with a greater accuracy of 1.75% of the reading and an absolute error of 0.1 l/min, it measures temperature from 0 to 50 °C at 1.75% of the reading and an absolute error of 0.5 °C and it can measure oxygen concentration with an accuracy of 1% [87]. For all tests the same test setup chain was used. This setup consisted of a ventilator with a flow regulated oxygen supply ,connected to a reference sensor, connected to our sensor, connected to a valve as shown in Figure 5.3. Depending on the test one of the two reference sensors was used and the valve used was a manually operated 600 WOG ball valve. For our sensor the 35° transducer angle was used as the default configuration if no other angle is noted.

5.6.1 Testing the oxygen sensing capability

The oxygen sensing capability of the sensor was first to be tested. The tests were performed at a constant flow through the sensor using a 35° transducer to flow angle, where the partial flow of oxygen was increased from atmospheric conditions by a flow regulated oxygen canister connected to the ventilator. Performing the test under constant flow rather than creating an enclosed volume of higher oxygen

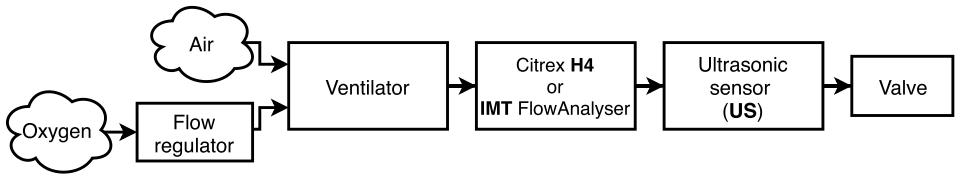

Figure 5.3: General test setup used to test out sensor. The ventilator is supplied with air and a regulated flow of oxygen, its output then goes through the reference sensor, into our sensor and finally through a valve to regulate the flow. Two different sensors were used as the reference, the Citrex H4 and the IMT FlowAnalyser. The valve used was a 600 WOG ball valve, except for the lung test where it was a 0.6 l lung simulator.

concentration is both easier and necessary with the reference sensors we are using as they require flow. Two different test series were performed, the first using the Citrex H4 as the reference at 30 l/min with an oxygen supply capable of supplying up to 6 l/min. The second test was performed using the IMT FlowAnalyser at 5, 15 and 50 l/min with an oxygen supply capable of supplying up to 15 l/min.

The first test, whose results are plotted in Figure 5.4, was performed at a constant flow of 30 l/min and a constant temperature of 24.4 °C for 300 s using the Citrex H4. The Citrex H4 was run at its maximum sample rate of 200 Hz and the additional oxygen flow started out at 0 l/min, increased to 1 l/min at 47 s, increased to 3 l/min at 118 s, increased to 6 l/min at 175 s and then decreased back to 0 l/min at 233 s. Comparing the concentration curves of the two sensors over time, it is clearly visible

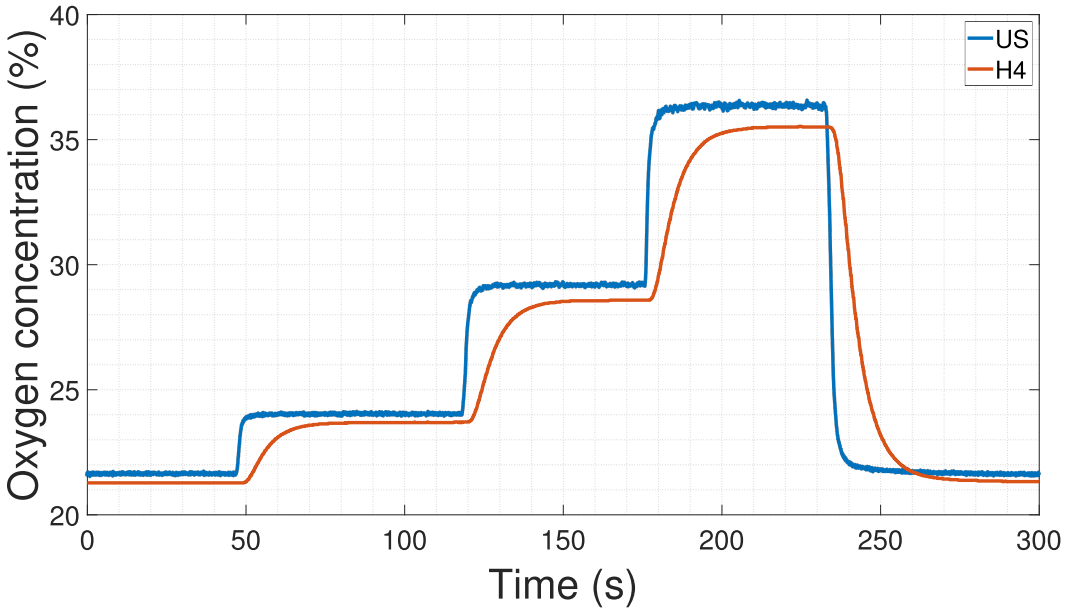

Figure 5.4: Concentration test curve showing the oxygen concentration measurements for both our ultrasonic sensor (US) and the Citrex H4 electrochemical sensor (H4) measuring the same flow. The curves are aligned in time making the difference in response time clear. The total flow was set to a constant rate of 30 l/min and the mixture of air and additional oxygen was varied stepped from 0 to 1, to 3, to 6 and back to 0 l/min.

that our ultrasonic sensor is reporting slightly higher values than the H4 electrochemical sensor and that the difference seems to increase with the concentration. A large difference in the response time is also made clear from our sensors almost vertical transitions to the H4 sensors slopes. Table 5.2 contains numerical comparisons of the two curves for the steady areas of each oxygen flow and for the 90% transition times to each flow. Difference is the comparison of the average value of the two sensors at each stable step.

Table 5.2: Table comparing the stable concentration averages of each oxygen flow tested in Figure 5.4 as well as the 90% transition times to each level from the previous one, for both sensors. US is our ultrasonic sensor and H4 is the Citrex H4. The flow column lists the partial flow of oxygen in the 30 l/min constant flow rate air and oxygen mixture.

Flow (l/min)	O_2 Concentration US (%)	O_2 Concentration H4 (%)	Difference (p.p.)	Rise/fall time US (s)	Rise/fall time H4 (s)
0	21.63	21.28	0.35	-	-
1	24.01	23.69	0.32	2.4	15.9
3	29.17	28.58	0.59	2.4	16.3
6	36.34	35.50	0.84	3.4	16.5
0	21.60	21.30	0.30	4.3	22.2

The second test series, using the IMT FlowAnalyser, was performed at constant flows of 5, 15 and 50 l/min with a partial oxygen flow of 0 to 15 l/min mixed into the air. The tests were performed at a temperature of 27 °C and the FlowAnalyser was run at 200 Hz. The different oxygen tank used in this test did not have discrete flow steps and as such the steps are not as evenly spaced and the changes between flows not as quick as the previous test using the H4. In the tests performed using the FlowAnalyser our sensor experienced noticeably more noise than when using the H4. This might have been caused by how much turbulence the two reference sensors induce on their outputs, as in both cases our sensor was connected to the output of the reference sensor. But ultimately we did not have enough time available using the FlowAnalyser to try and identify why this measurement series had more noise.

The first FlowAnalyser test was performed at 5 l/min and is shown in Figure 5.5. The measurement starts with only air, where the measured concentration difference between our sensor and the FlowAnalyser is about 0.1 p.p.. As the oxygen concentration increases as more oxygen is added, our sensor reports slightly larger values, with a peak difference of about 0.7 p.p. above the FlowAnalyser. They converge again at 88% and our sensor ends up about 0.8 p.p. below the FlowAnalyser as it reports 100%. The total span of difference between the two sensors is about 1.5 p.p.. The measured flow is also included in this figure to show that there is a small decrease in the measured flow as well as a small increase in noise when approaching 80% concentration. This effect was only seen at low flows and it was not possible to tell to which extent it was due to environmental factors changing as the ventilator went from sucking in air to having oxygen blown in already at the target pressure.

The second FlowAnalyser test was performed at the slightly higher 15 l/min and is shown in Figure 5.6. Like the first measurement it starts with only air, where our sensor reports a value about 0.25 p.p. above the FlowAnalyser. Again as the

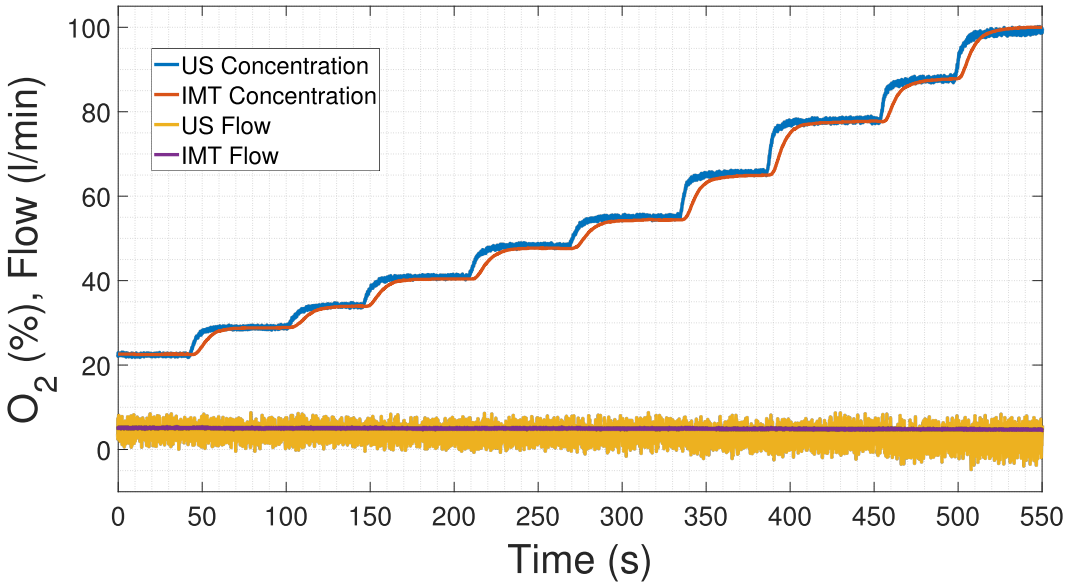

Figure 5.5: Concentration test curve showing the oxygen concentration measurements for both our ultrasonic sensor (US) and the IMT FlowAnalyser (IMT) measuring the same flow. The curves are aligned in time making the difference in response time clear. The total flow was set to a constant rate of 5 l/min and the mixture of air and additional oxygen was varied by stepping the oxygen component of the flow from 0 to 5 l/min. The measured flow is included in this figure to show that there is a small decrease in the measured flow as well as a small increase in noise when approaching 80% concentration.

concentration increases our sensor reports slightly higher values of up to about 1.2 p.p. to then converge back at 100%.

The third and final FlowAnalyser test was performed at 50 l/min, to complete the series with a measurement of a flow higher than the tests with the H4 sensor. It is shown in Figure 5.7 and here our sensor started out about 0.5 p.p. below the FlowAnalyser, to converge at middle of the range tested, 33%, and then finish about 0.6 p.p. above at the maximum concentration of 47.7%. This gives a total span of difference of about 1.5 p.p., though the maximum concentration is limited to what is reachable from by 15 l/min of oxygen in a 50 l/min flow.

5.6.2 Testing the flow sensing capability

To test the flow sensing capability of the sensor, tests were performed using the same test setup as the oxygen test, with a ventilator to provide flow and the Citrex H4 as the reference sensor. No oxygen was added to the flow in this test, but multiple tests were performed using all three available transducer angles (35°, 55° and 75° to the flow) in both directions. Before each test the sensor was calibrated to the current angle and distance using the method previously described in Section 5.4. The distance between the transducer also changes with the angle, to keep them at the edge of the flow path, the distance between the back ends of the transducer

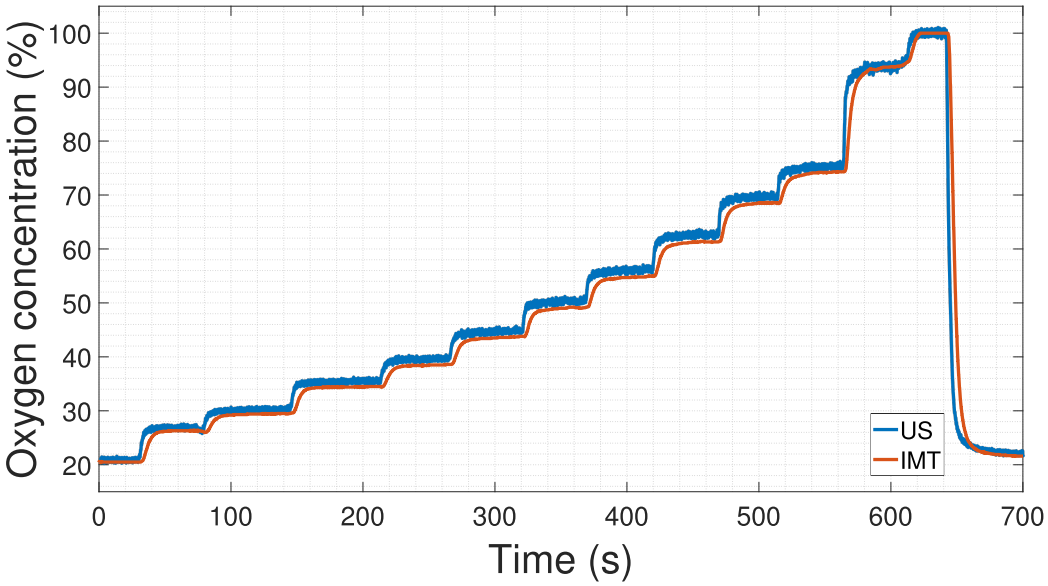

Figure 5.6: Concentration test curve showing the oxygen concentration measurements for both our ultrasonic sensor (US) and the IMT FlowAnalyser (IMT) measuring the same flow. The curves are aligned in time making the difference in response time clear. The total flow was set to a constant rate of 15 l/min and the mixture of air and additional oxygen was varied by stepping the oxygen component of the flow from 0 to 15 l/min.

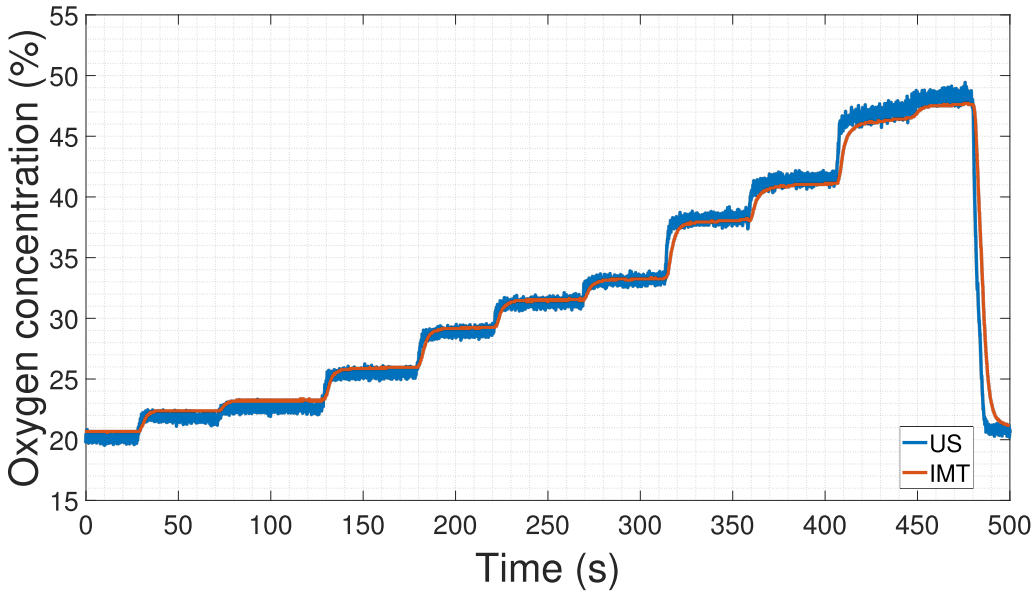

Figure 5.7: Concentration test curve showing the oxygen concentration measurements for both our ultrasonic sensor (US) and the IMT FlowAnalyser (IMT) measuring the same flow. The curves are aligned in time making the difference in response time clear. The total flow was set to a constant rate of 50 l/min and the mixture of air and additional oxygen was varied by stepping the oxygen component of the flow from 0 to 15 l/min.

pair was 49 mm for 35°, 42 mm for 55° and 32 mm for 75°. Part of the forward direction tests of each angle is plotted in Figures 5.8, 5.9 and 5.10. The results of the tests in the reverse direction are available in appendix II as no major differences were observed based on the direction. As the flow variation was performed using a manually operated valve, there is some variation in the duration and the steps of the different flows tested.

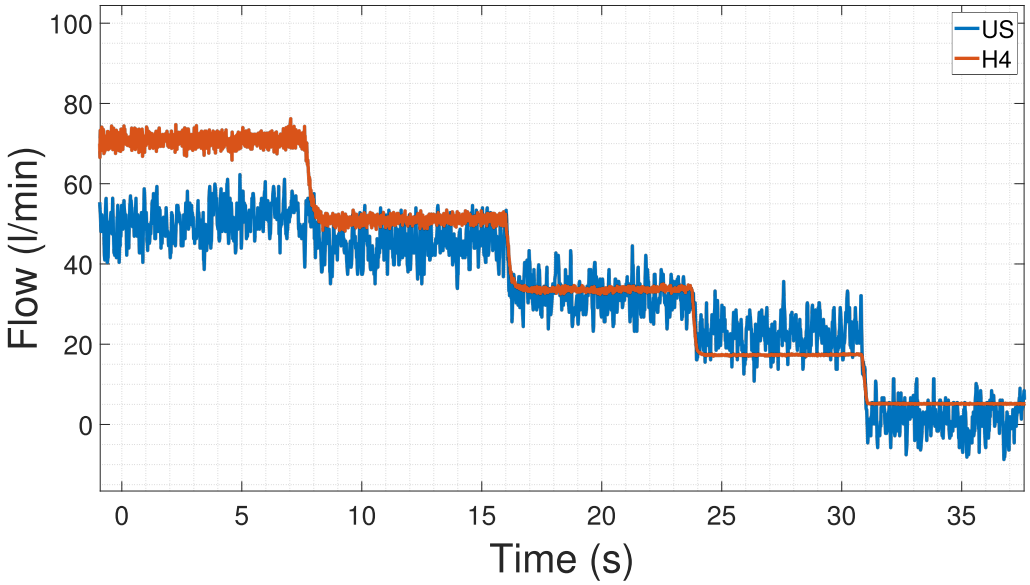

Figure 5.8: Flow test with 75° transducer angle at 32 mm distance in forward direction.

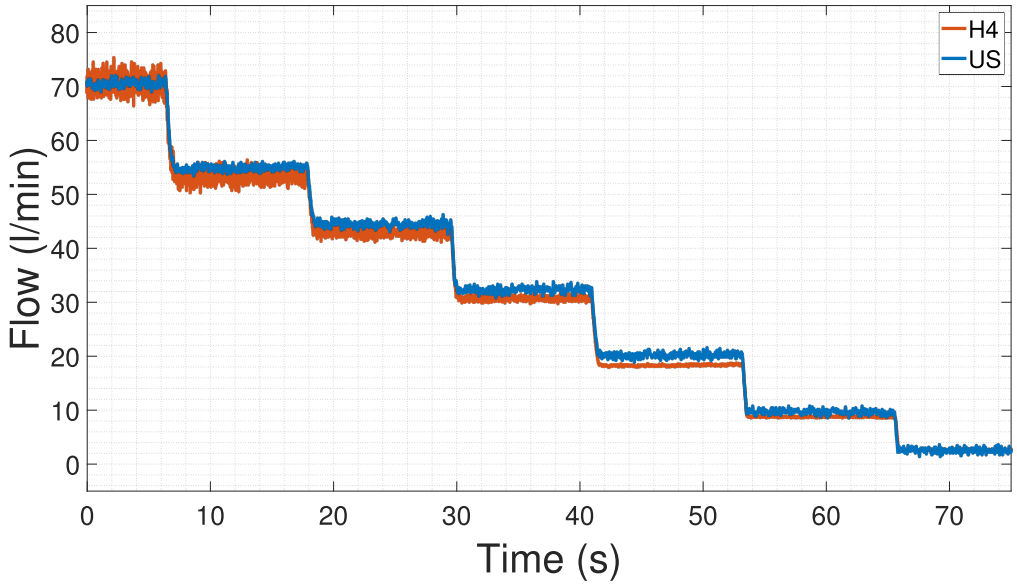

Figure 5.9: Flow test with 55° transducer angle at 42 mm distance in forward direction.

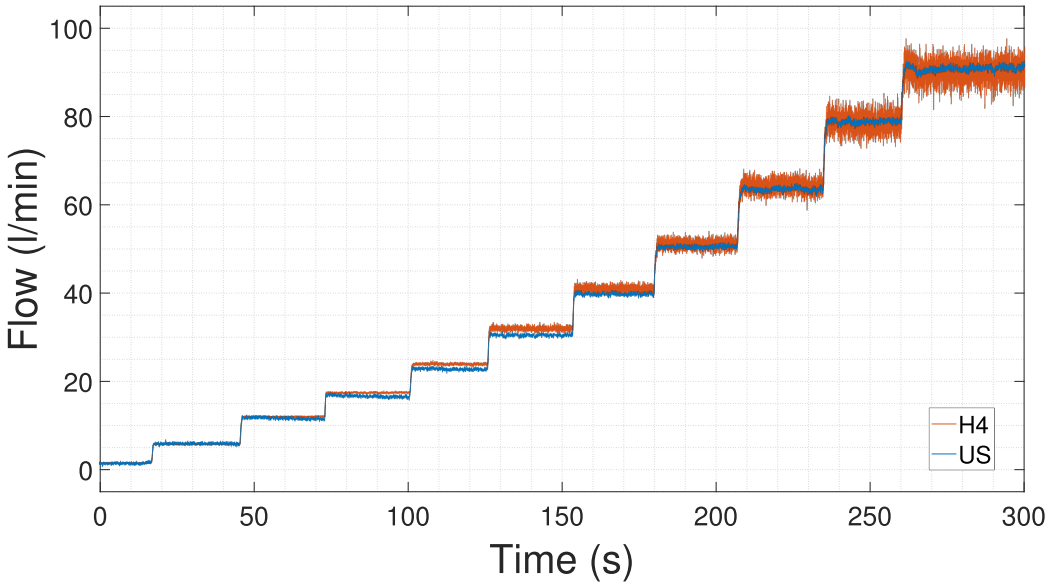

Figure 5.10: Flow test with 35° transducer angle at 49 mm distance in forward direction.

Figure 5.8 shows the flow plot of the steepest angle. This angle was, as mentioned in Section 4.7, included as it has been reported to be optimal in liquids to minimise the impact of turbulence. But as expected the geometry of such a steep angle also has a clear negative impact by shrinking the flow component of the TOF as well as lowering the distance between the transducers. The resulting measurement is both extremely noisy with a standard deviation of 4 l/min and a mean of 45 l/min at the 50 l/min step of the H4. It also has a very clear and large non-linear error against the Citrex H4.

Proceeding to the middle angle of 55° in Figure 5.9, the signal of our sensor becomes much clearer as the angle becomes slightly more shallow and the distance between the transducers slightly longer. At the 43 l/min step of the H4 our sensor has a slightly larger mean of 44.4 l/min but a standard deviation of only 0.5 l/min, slightly lower than the H4 at 0.63 l/min. It can also be seen that in this configuration our sensor is more noisy than the H4 at low flows, but less noisy at high flows. There is still some non-linear error, but it is again smaller than that of the 75° configuration.

The final angle, 35°, is both the most shallow angle and the longest measurement distance. It also has the best performance of the three angles in exchange for the larger space required between the transducers. Comparing the sensor readout to the H4 at the 40.9 l/min step, our sensor reports a mean of 39.7 l/min, while our sensor has a standard deviation of 0.28 l/min and the H4 has 0.57 l/min. Like before our sensor is much less noisy at high flows, but it is still noisier than the H4 at low flows. There is still some error across the range, reaching a maximum of about 1.3 l/min at the 31.7 l/min step.

The flow response time of the sensor in our tests was observed to be as quick as the H4, at around 0.5 s. This is low enough that the transition time of manually turning

the valve most likely makes up a sizeable part of the total time.

To complement the tests of our sensor performing at different flow rates the 35° angled transducer was run at the maximum achievable flow, 290 l/min, in both directions using air to verify that this would not push the flow past the maximum limits for selecting the TOF pulse as described in Section 5.3, which was estimated to 420 l/min without temperature compensation. This test was performed successfully at 29 °C without observing any incorrect values giving us a known working maximum for all lower temperatures and higher oxygen concentrations.

5.6.3 Testing the sensor with a lung simulator

We were able to test our sensor on a ventilator connected to a 0.6 l lung simulator together with the IMT FlowAnalyser. This was done with 11 l/min oxygen supplied in the ventilator flow and with a leakage between the sensors and the lung of 16 l/min. A diagram of the test setup is shown in figure 5.3, where the valve was replaced with the simulator, and the resulting plot of flow and oxygen concentration is shown in Figure 5.11. The flow of our sensor mirrors that of the FlowAnalyser well albeit with more noise. We are not able to directly compare the oxygen concentration between our sensor and the FlowAnalyser due to the large difference in response time. But we can see that as the lung expires gas (flow below 16 l/min) the concentration stays mostly constant, this is expected as the constant flow of now would be flowing away from the sensor rather than through it. As the expiration ends and the flow direction reverts, the concentration starts to increase as the added oxygen makes up a large part of the 16 l/min leakage flow. Then as the inspiration starts the concentration drops again as the flow rapidly increases and the oxygen makes a smaller part of the flow.

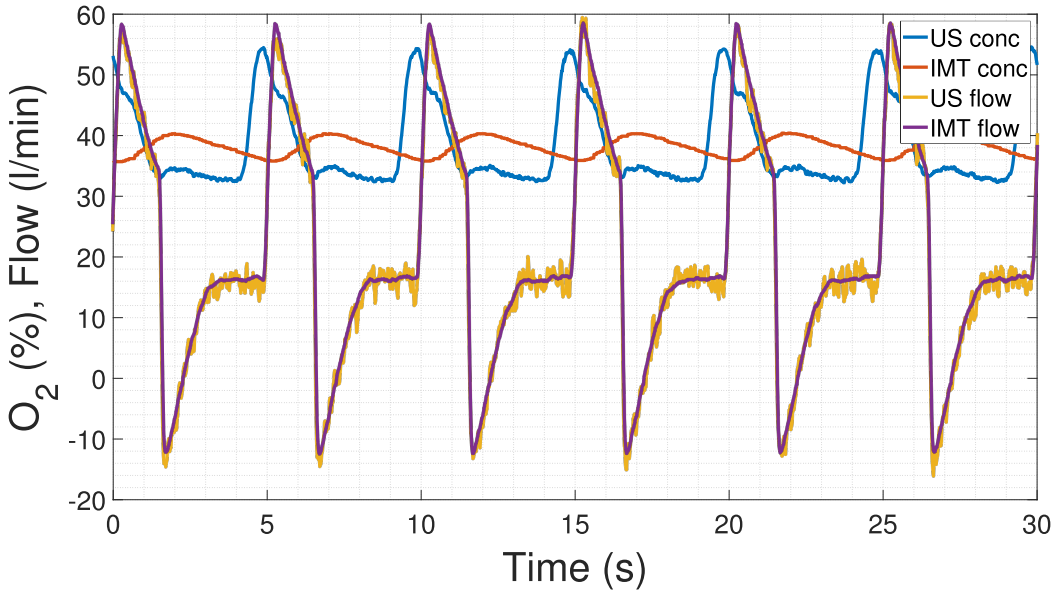

Figure 5.11: Flow and concentration test with a 0.6 l lung simulator. The output of our sensor (US) was connected to lung simulator and the input to the IMT FlowAnalyser output. The FlowAnalyser input was connected to the ventilator.

6

Conclusion

This final chapter includes a discussion of the results in relation to previously set requirements and other measures that we found relevant. The discussion part is then followed by the conclusion that gives a final overview of the results.

6.1 Discussion

Earlier in the report (Section 2.3) we brought up different advantages ultrasonic gas sensors have over other (but mainly electrochemical) gas sensors such as longer lifetime, no secondary pollution, high accuracy and linearity, quick response time and low price. We also discussed some possible disadvantages such as low selectivity and the sensors being limited to binary and pseudo-binary gas mixtures. Additionally, we talked about using the sensor as a flow meter (Section 2.4), with the advantages being absence of moving parts and pressure drop, as well as the sensor's insensitivity to gas composition fluctuation and bi-directional flow measurement possibility.

During our work we evaluated the performance-related claims of using the sensor for both oxygen concentration measurement and flow measurement to see if they apply to our sensor as well and if it would be an improvement from the previously used one.

To start with advantages we tested the accuracy, linearity and response time of the oxygen concentration measurement. Table 5.2 in Section 5.6.1 shows that compared to the sensor we had as a reference the maximum difference of our sensor was within 1.2 p.p.. However, as mentioned in Section 5.6 the reference sensors have an accuracy of 1%, which still means that the developed sensor is in line with the accuracy requirement that was set in the beginning of $\pm$(2.5% + 2.5% of gas concentration) as the bigger differences are seen at higher concentrations, where 2.5% of the gas concentration is enough to raise the accuracy requirement to 3% of overall range. Regarding the response time, because of how the oxygen concentration was changed (using a manually turned valve), it is not possible to find the absolute response time, however, it is possible to compare the rise times of our sensor to the reference sensor Citrix H4. As shown in Table 5.2 in Section 5.6, the difference between rise/fall time between two sensor shows that our sensor can be as much as 6.8 times quicker.

For flow-meter operation of the sensor we showed that it can successfully measure the flow in both directions (Section 5.6.2). From Figure 5.5 it can also be seen how

the oxygen concentration does not affect the flow measurement, as we can see the flow remains constant as the oxygen concentration is increased. Section 5.6.2 showed that from three transducer angles tested, 35° gave the most accurate results with the maximum difference compared to the reference sensor being 1.3 l/min at 31.7 l/min, when compared to the requirements of ±(2.5% + 0.5% of the measurement range (assumed to be at 300 l/min)) which would give us the range of ± 2.29 l/min, it is clear that our flow sensor is well inside the allowed error.

As mentioned in Section 5.6.2 the maximum flow we could test through the system was 290 l/min at 29 °C and while this was successful, it is lower than the requirement (400 l/min at 40 °C) that was set in the beginning of development. Because we did not have the possibility of testing with any higher flow it is not possible to say if the system fulfills this requirement or not. But the system's theoretical operating limits are from 420 l/min without to 725 l/min with temperature compensation and the verified 290 l/min is nonetheless an increase from the sensor currently used in the ventilators we have been using for flow generation which are limited to measuring 250 l/min. The flow measurement is also directly dependent on the diameter of the flow path through the sensor as described by (2.13) and as such increasing the diameter would also increase the maximum flow. The flow meter response time also does not fulfill the requirement, as explained in Section 5.5, to keep the maximum measurement deviation lower than 1 l/min the sample duration has to be at least 7 ms, which means that the measurement duration is 14 ms and with the four sample moving average filter the response time becomes 60 ms.

However, there are also some important disadvantages to the system, the previously mentioned non-selectivity being the biggest one of them. The non-selectivity means that for accurate measurements oxygen can be the only component of air that is changing. Having unexpected gases present or concentrations of other components in the air changing, is a possible threat to the user of the ventilator which could receive too much or too little oxygen as a result of it. Another disadvantage is that the device does require precise calibration. As mentioned in Section 5.4 the oxygen concentration calculation is highly dependent on the distance between the transducers. Although the distance is not only related to physical distance but adjusted to include other delays, even only a small change in distance results in a big change in calculated oxygen concentration. This means that the sensor might even need to actively compensate its calibration because temperature changes cause the tube material to expand and contract, depending on the thermal expansion coefficients of the materials used. Selecting correct materials for the pipe and the pipe-transducer connection can decrease the expansion and contraction effect on the sensor. An upside to the calibration is that except for requiring two points of known oxygen-air mixtures, it requires no additional external precision measurements to be done of the sensor and could as such be implemented as a software calibration routine.

Finally, to address rest of the system requirements we set in Section 1.4, it is possible to say that we fulfilled most of the requirements. The PCB is well within the size requirements (37.5 x 56 x 14 mm), while the transducers are meant to be integrated to the existing pipes without adding much additional volume either. Furthermore,

it is possible to make the PCB even smaller, as depending on the integrated system, the power conversion is expected to not be needed with the correct voltage level coming from within the larger system. Additionally, the board can also be scaled down if hand-soldering the board is not required. This scaling, however, would require careful design considerations to make sure that the changing layout would not induce additional noise in the system.

To fulfill the temperature and humidity requirements, suitable components were chosen, though neither temperature nor high humidity testing was performed to evaluate component lifetimes. The operating pressure range was also not tested, however, the concentration and flow speed measurements are not affected by the pressure, as (2.3) shows that the speed of sound equation in an ideal gas does not have the pressure component. The final requirement was related to operating voltages, and although our system needs -5 V, which is not available from the system, we have included a voltage converter in our design that is converting 5 V to -5 V.

6.2 Conclusion

As a result of this Master's thesis project an ultrasonic oxygen sensor for oxygen concentration and flow measurement in a ventilator device was developed. The proposed sensor design is a potential replacement for the right now widely used electrochemical oxygen sensor, as it is quicker, cheaper, more environmentally friendly and can also measure flow in addition to measuring oxygen concentration.

The system design includes a hardware solution (PCB), a software solution for interpreting the signals received and a possible mechanical design. These parts were integrated with an already existing system that provided the MCU.

Testing and verification was done with existing medical ventilators and the system was both calibrated and compared to the Citrex H4 and the IMT FlowAnalyser. The test results showed that the oxygen concentration measurements of the developed sensor were indeed multiple times quicker than the reference sensors. Furthermore, the accuracy of both the concentration sensor and flow meter was within the required range.

The only disadvantages of the system are the non-selectivity of the sensor and the need for precise calibration.

So a working sensor has been developed and while further development and testing is required to reach a product which is suitable for a medical environment, a point has been reached where it shows promising performance in accuracy and range for measuring both oxygen concentration and flow.

Bibliography

[1] General Electric Co, "Apparatus for measuring the density of gases," 1942.

[2] U. S. Airforce, *Ultrasonic Oxygen Sensor*. USAF School of Aerospace Medicine, 1987.

[3] World Health Organization, "Chronic obstructive pulmonary disease (COPD)," December 2017. [Online]. Available: https://www.who.int/en/news-room/fact-sheets/detail/chronic-obstructive-pulmonary-disease-(copd) [Accessed: 15/05/2019]

[4] World Health Organization, *Global surveillance, prevention and control of chronic respiratory diseases*. World Health Organization, 2007.

[5] E. R. Society, *Forum of International Respiratory Societies. The Global Impact of Respiratory Disease – Second Edition*. European Respiratory Society, 2017.

[6] R. Lauber, A. Steiner, and A. M. Zbinden, "Accuracy, alarm limits and rise times of 12 oxygen analysers," *Anaesthesia*, vol. 49, no. 12, pp. 1071–1077, 1994.

[7] IT Dr. Gambert GmbH, "O2 - Medical Sensor / Type M-03," 2014. [Online]. Available: http://www.it-wismar.de//_documents/specs/M-03_spec.pdf [Accessed: 15/05/2019]

[8] IT Dr. Gambert GmbH, "O2 - Gas Sensors containing KOH and Lead," Feb 2002. [Online]. Available: http://www.it-wismar.de/download.php?id=136 [Accessed: 15/05/2019]

[9] Wuhan Cubic Optoelectronics Co., Ltd., *Ultrasonic Oxygen Sensor Module Gasboard7500C*. Wuhan Cubic Optoelectronics Co., Ltd., 2018.

[10] G. Brooker, *Introduction to Biomechatronics*. SciTech Publishing, 2012.

[11] Drägerwerk AG & Co. KGaA, *The History of Dräger*. Drägerwerk AG & Co. KGaA, 2010. [Online]. Available: https://www.draeger.com/Corporate/Content/the_history_of_draeger_2.pdf

[12] G. D. Baura, *Medical Device Technologies - A Systems Based Overview Using Engineering Standards*. Elsevier, 2012. [Online]. Available: https://app.knovel.com/hotlink/toc/id:kpMDTASBO3/medical-device-technologies/medical-device-technologies

[13] D. J. Baker, *Artificial Ventilation : A Basic Clinical Guide.* Springer, 2016.

[14] CDC/GHO/M. Hilpertshauser, "File:iron lung cdc.jpg - wikimedia commons," 2006. [Online]. Available: https://commons.wikimedia.org/wiki/File:Iron_lung_CDC.jpg [Accessed: 15/05/2019]

[15] S. Bellini, "File:bird mark 8 medical respirator1.jpg - wikimedia commons," 2015. [Online]. Available: https://commons.wikimedia.org/wiki/File:Bird_Mark_8_Medical_respirator1.JPG [Accessed: 15/05/2019]

[16] Drägerwerk AG & Co. KGaA, "Oxygen sensor capsule," 2019. [Online]. Available: https://www.draeger.com/en_uk/Hospital/Products/Accessories-and-Consumables/Sensors/Oxygen-Sensor-Capsule [Accessed: 15/05/2019]

[17] Nuova GmbH, "Medical oxygen sensors | nuova gmbh medical division," 2019. [Online]. Available: https://www.nuova.de/en/medical-oxygen-sensors.html [Accessed: 15/05/2019]

[18] Magnamed, "Babymag," 2019. [Online]. Available: http://www.magnamed.com.br/content/arquivos/de2415c41efc7b572e73c8de4b14dd2c.pdf [Accessed: 15/05/2019]

[19] Heinen + Löwenstein, "Charisma high-flow cpap solution," 2016. [Online]. Available: https://hul.de/wp-content/uploads/2016/05/Charisma-EN-Ansicht.pdf [Accessed: 15/05/2019]

[20] P. T. Meriläinen, "A differential paramagnetic sensor for breath-by-breath oximetry." *Journal Of Clinical Monitoring*, vol. 6, no. 1, pp. 65 – 73, 1990.

[21] Fisher & Paykel, "Airvo™ 2 humidification system," 2019. [Online]. Available: https://www.fphcare.com/nz/hospital/adult-respiratory/optiflow/airvo-2-system/ [Accessed: 15/05/2019]

[22] UTAS Co., "Uvent t," 2019. [Online]. Available: http://www.utasco.com/en/dykhatelnaya-apparatura-2/uvent-t7 [Accessed: 15/05/2019]

[23] Maquet, "Servo-s v8.0 data sheet," 2016. [Online]. Available: https://www.getinge.com/siteassets/products-a-z/servo-s-mechanical-ventilator/lab-6670115---05.00---servos_data_6670115_r15_160318_en_nonus12.pdf?disclaimerAccepted=yes [Accessed: 15/05/2019]

[24] C. for Chemical Process Safety, *Continuous Monitoring for Hazardous Material Releases.* Center for Chemical Process Safety/AIChE, 2009. [Online]. Available: https://app.knovel.com/hotlink/toc/id:kpCMHMR005/continuous-monitoring/continuous-monitoring

[25] M. Willett, "Oxygen sensing for industrial safety — evolution and new approaches," *Sensors*, vol. 14, no. 4, pp. 6084–6103, 2014.

[26] G. Sberveglieri, *Gas Sensors: Principles, Operation and Developments.* Dordrecht : Springer Netherlands : Imprint: Springer, 1992.

[27] R. V. Harrison, *Chemical sensors: properties, performance, and applications.* New York : Nova Science Publishers, 2010.

[28] R. Jaaniso, *Semiconductor gas sensors.*, ser. Woodhead publishing series in electronic and optical materials: number 38. Oxford : Woodhead Publishing, 2013.

[29] R. Ramamoorthy, P. K. Dutta, and S. A. Akbar, "Oxygen sensors: Materials, methods, designs and applications," *Journal of Materials Science*, vol. 38, no. 21, pp. 4271–4282, Nov 2003.

[30] R. E. Hetrick, W. A. Fate, and W. C. Vassell, "Oxygen sensing by electrochemical pumping," pp. 390–392, 1981. [Online]. Available: https://doi.org/10.1063/1.92349

[31] L. Xiong and R. G. Compton, "Amperometric gas detection: A review," 2014.

[32] S. V. Hatch, *Computerized Engine Controls (9th Edition).* Cengage Learning, Inc., 2012. [Online]. Available: https://app.knovel.com/hotlink/toc/id:kpCECE0001/computerized-engine-controls/computerized-engine-controls

[33] D. Kuhlgatz, "40 Years of Bosch Lambda Sensor," 2016. [Online]. Available: https://blog.bosch.com/history/en/2016/07/20/939/ [Accessed: 15/05/2019]

[34] W. Nawrocki, *Measurement Systems and Sensors (2nd Edition).* Artech House, 2016. [Online]. Available: https://app.knovel.com/hotlink/toc/id:kpMSSE0013/measurement-systems-sensors/measurement-systems-sensors

[35] C. Cobianu, B. Serban, V. Avramescu, B. Hobbs, K. Pratt, and M. Willett, "Lead-free galvanic oxygen sensors — a conceptual approach," in *CAS 2012 (International Semiconductor Conference)*, vol. 1, Oct 2012, pp. 161–164.

[36] W. Boyes, *Instrumentation Reference Book (4th Edition).* Elsevier, 2010. [Online]. Available: https://app.knovel.com/hotlink/toc/id:kpIRBE0016/instrumentation-reference/instrumentation-reference [Accessed: 15/05/2019]

[37] L. Pauling, R. E. Wood, and J. H. Sturdivant, "An instrument for determining the partial pressure of oxygen in a gas1," *Journal of the American Chemical Society*, vol. 68, no. 5, pp. 795–798, 1946. [Online]. Available: https://doi.org/10.1021/ja01209a029

[38] J. Lauer, *Sensors for Gas Phase Oxygen Analysis.* Teledyne analytical instruments, 2002. [Online]. Available: http://www.teledyne-ai.com/pdf/lauer.pdf

[39] B. Eckstein, "Paramagnetic o2," 2019. [Online]. Available: https://www.anandic.com/en/Training-Center/Parameter-Technology/Paramagnetic-O2/page40752.htm [Accessed: 15/05/2019]

[40] V. Magori, "Ultrasonic sensors in air," in *1994 Proceedings of IEEE Ultrasonics Symposium*, vol. 1, Oct 1994, pp. 471–481 vol.1.

[41] S. Jacobson, "New developments in ultrasonic gas analysis and flowmetering," in *2008 IEEE Ultrasonics Symposium*, Nov 2008, pp. 508–516.

[42] A. J. Zuckerwar, *Handbook of the Speed of Sound in Real Gases.*, ser. Handbook of the Speed of Sound in Real Gases. Academic Press, 2002, no. Volume III, Speed of sound in air.

[43] X. Liu, S. Cheng, H. Liu, S. Hu, D. Zhang, and H. Ning, "A survey on gas sensing technology," *Sensors (Basel, Switzerland)*, vol. 12, pp. 9635–65, 12 2012.

[44] C. Nordling and J. Österman, *Physics Handbook for Science and Engineering.* Studentlitteratur, 2006.

[45] P. Atkins and L. Jones, *Chemical Principles.* W. H. Freeman and Company, 2008.

[46] S. Minglei, L. Xiang, Z. Changping, and Z. Jiahua, "Gas concentration detection using ultrasonic based on wireless sensor networks," in *The 2nd International Conference on Information Science and Engineering*, Dec 2010, pp. 2101–2106.

[47] A. Petculescu and R. M. Lueptow, "Quantitative acoustic relaxational spectroscopy for real-time monitoring of natural gas: A perspective on its potential," *Sensors and Actuators B: Chemical*, vol. 169, pp. 121 – 127, 2012. [Online]. Available: http://www.sciencedirect.com/science/article/pii/S0925400512003589

[48] A. Petculescu, B. Hall, R. Fraenzle, S. Phillips, and R. M. Lueptow, "A prototype acoustic gas sensor based on attenuation," *The Journal of the Acoustical Society of America*, vol. 120, no. 4, pp. 1779–1782, 2006. [Online]. Available: https://doi.org/10.1121/1.2336758

[49] S. G. Ejakov, S. Phillips, Y. Dain, R. M. Lueptow, and J. H. Visser, "Acoustic attenuation in gas mixtures with nitrogen: Experimental data and calculations," *The Journal of the Acoustical Society of America*, vol. 113, no. 4, pp. 1871–1879, 2003. [Online]. Available: https://doi.org/10.1121/1.1559177

[50] W. Hennessy, "A review of your flow sensing options," 2006. [Online]. Available: https://www.sensorsmag.com/components/a-review-your-flow-sensing-options

[51] P. Brassier, B. Hosten, and F. Vulovic, "High-frequency transducers and correlation method to enhance ultrasonic gas flow metering," *Flow Measurement and Instrumentation*, vol. 12, no. 3, pp. 201 – 211, 2001. [Online]. Available: http://www.sciencedirect.com/science/article/pii/S0955598601000139

[52] T. Wang, J. Wang, F. Ren, and Y. Jin, "Application of doppler ultrasound velocimetry in multiphase flow," *Chemical Engineering Journal*, vol. 92, no. 1, pp. 111 – 122, 2003. [Online]. Available: http://www.sciencedirect.com/science/article/pii/S1385894702001286

[53] Honeywell, "Mass flow sensors: Mass flow versus volumetric flow and flow rate unit conversions," 2012. [Online]. Available: https://sensing.honeywell.com/mass-flow-vs-volumetric-flow-and-unit-conversion-tn-008043-2-en-final-06nov12.pdf [Accessed: 15/05/2019]

[54] The Editors of Encyclopaedia Britannica, *Amplifier*. Chicago, IL, USA: Encyclopædia Britannica, inc., 2009. [Online]. Available: https://www.britannica.com/technology/amplifier

[55] H. S. Black, "Stabilized feed-back amplifiers," *Proceedings of the IEEE*, vol. 87, no. 2, pp. 379–385, Feb 1999.

[56] P. Horowitz and W. Hill, *The Art of Electronics*, 3rd ed. New York, NY, USA: Cambridge University Press, 2015.

[57] C. Psoc, P. Acevedo, M. Fuentes, J. Durán, M. Vázquez, and C. Díaz, "Pulse Generator for Ultrasonic Piezoelectric Transducer Arrays Based on a Programmable System-on-," *Advances in Science, Technology and Engineering Systems Journal*, vol. 2, no. 3, pp. 205–209, 2017. [Online]. Available: https://astesj.com/v02/i03/p27/

[58] Analog Devices, "Ad8033/ad8034," 2008. [Online]. Available: https://www.analog.com/media/en/technical-documentation/data-sheets/AD8033_8034.pdf [Accessed: 15/05/2019]

[59] R. Mancini, "Op amps for everyone," Dallas, TX, USA, 2002. [Online]. Available: https://web.mit.edu/6.101/www/reference/op_amps_everyone.pdf [Accessed: 15/05/2019]

[60] M. Duff, "how to calculate the required gbw with analog filter wizard?" 2017. [Online]. Available: https://ez.analog.com/amplifiers/operational-amplifiers/f/q-a/16811/how-to-calculate-the-required-gbw-with-analog-filter-wizard [Accessed: 15/05/2019]

[61] U. Beis, "Design and dimensioning of active filters," 2015. [Online]. Available: https://www.beis.de/Elektronik/Filter/Filter.html [Accessed: 15/05/2019]

[62] A. Devices, "Selection table for operational amplifiers (op amps)," 2019. [Online]. Available: https://www.analog.com/en/parametricsearch/11070#/ [Accessed: 15/05/2019]

[63] Analog Devices, "Lt1711/lt1712," 2001. [Online]. Available: https://www.analog.com/media/en/technical-documentation/data-sheets/171112f.pdf [Accessed: 15/05/2019]

[64] Texas Instruments, "Filterpro user's guide," 2011. [Online]. Available: http://www.ti.com/lit/an/sbfa001c/sbfa001c.pdf [Accessed: 15/05/2019]

[65] National Semiconductor Corporation, "A basic introduction to filters - active, passive, and switched-capacitor," 2010. [Online]. Available: http://www.ti.com/lit/an/snoa224a/snoa224a.pdf [Accessed: 15/05/2019]

[66] H. Zumbahlen, "Mini tutorial: Sallen-key filters," 2017. [Online]. Available: https://www.analog.com/media/en/training-seminars/tutorials/MT-222.pdf [Accessed: 15/05/2019]

[67] Maxim Integrated Products, Inc, "A beginner's guide to filter topologies," 2003. [Online]. Available: https://www.maximintegrated.com/en/app-notes/index.mvp/id/1762 [Accessed: 15/05/2019]

[68] H. Zumbahlen, "Mini tutorial: Multiple feedback filters," 2012. [Online]. Available: https://www.analog.com/media/en/training-seminars/tutorials/MT-220.pdf [Accessed: 15/05/2019]

[69] P. Brassier, B. Hosten, and F. Vulovic, "High-frequency transducers and correlation method to enhance ultrasonic gas flow metering," *Flow Measurement and Instrumentation*, vol. 12, no. 3, pp. 201 – 211, 2001. [Online]. Available: http://www.sciencedirect.com/science/article/pii/S0955598601000139

[70] B. Hök, A. Blückert, and J. Löfving, "Acoustic gas sensor with ppm resolution," *Sensor Review*, vol. 20, no. 2, pp. 139–142, 2000. [Online]. Available: https://doi.org/10.1108/02602280010319231

[71] Analog Devices, "LTSpice." [Online]. Available: https://www.analog.com/en/design-center/design-tools-and-calculators/ltspice-simulator.html [Accessed: 15/05/2019]

[72] Analog Devices, "Analog filter wizard." [Online]. Available: https://www.analog.com/designtools/en/filterwizard/ [Accessed: 15/05/2019]

[73] Texas Instruments, "Filter design tool." [Online]. Available: http://www.ti.com/design-tools/signal-chain-design/webench-filters.html [Accessed: 15/05/2019]

[74] STMicroelectronics, "Stm32f765xx stm32f767xx stm32f768ax stm32f769xx datasheet - production data," 2017. [Online]. Available: https://www.st.com/resource/en/datasheet/stm32f765bg.pdf [Accessed: 15/05/2019]

[75] Murata, "Ultrasonic sensor application manual," 2008. [Online]. Available: http://www.ee.columbia.edu/~kinget/EE6350_S14/DM6350_web/files/murata.pdf [Accessed: 15/05/2019]

[76] ON Semiconductor, "Inverting buffer / cmos logic level shifter," 2016. [Online]. Available: https://www.onsemi.com/pub/Collateral/MC74VHC1GT04-D.PDF [Accessed: 15/05/2019]

[77] Multicomp, "Surface Mount Resistor Kit, 0603 Case Size," 2015. [Online]. Available: http://www.farnell.com/datasheets/1895129.pdf [Accessed: 02/07/2019]

[78] Panasonic, "Stacked Metallized PPS Film Chip Capacitor," 2017. [Online]. Available: https://industrial.panasonic.com/cdbs/www-data/pdf/RDI0000/ABD0000C173.pdf [Accessed: 02/07/2019]

[79] Murata Power Solutions, "8200 Series Miniature Surface Mount Power Inductors," 2011. [Online]. Available: https://www.murata-ps.com/pub/data/magnetics/kmp_8200c.pdf [Accessed: 02/07/2019]

[80] Murata, "MEA1 Series," 2018. [Online]. Available: https://power.murata.com/pub/data/power/ncl/kdc_mea.pdf [Accessed: 15/05/2019]

[81] STMicroelectronics, "Rm0410 reference manual," 2018. [Online]. Available: https://www.st.com/content/ccc/resource/technical/document/

reference_manual/group0/96/8b/0d/ec/16/22/43/71/DM00224583/files/DM00224583.pdf/jcr:content/translations/en.DM00224583.pdf [Accessed: 15/05/2019]

[82] F. J. Weber, "Ultrasonic beam propagation in turbulent flow," Ph.D. dissertation, Worcester Polytechnic Institute, 100 Institute Rd, Worcester, MA 01609, USA, 12 2003.

[83] Texas Instruments, "Tdc1000 ultrasonic sensing analog front end," Dallas, TX, USA, 2014. [Online]. Available: http://www.ti.com/lit/ds/symlink/tdc1000.pdf [Accessed: 24/05/2019]

[84] Texas Instruments, "Tdc1000 ultrasonic sensing analog front end," Dallas, TX, USA, 2016. [Online]. Available: http://www.ti.com/lit/ds/symlink/tdc7200.pdf [Accessed: 24/05/2019]

[85] Murata, "MA40S4S Data Sheet," 2015. [Online]. Available: https://www.murata.com/products/en-sg/products/productdata/8797589340190/MASPOPSE.pdf [Accessed: 15/05/2019]

[86] imtmedical ag, *User Manual CITREX H4*. imtmedical ag, 2018. [Online]. Available: http://imtmedical.pl/download/Citrex%20H4/CITREX%20H4%20-%20Instrukcja%20Obslugi%20EN.pdf

[87] imtmedical ag, "Flowanalyser PF300 Specification," 2018. [Online]. Available: https://www.imtanalytics.com/Analyser/FlowAnalyser_Specification [Accessed: 22/05/2019]

A

Appendix: Schematic

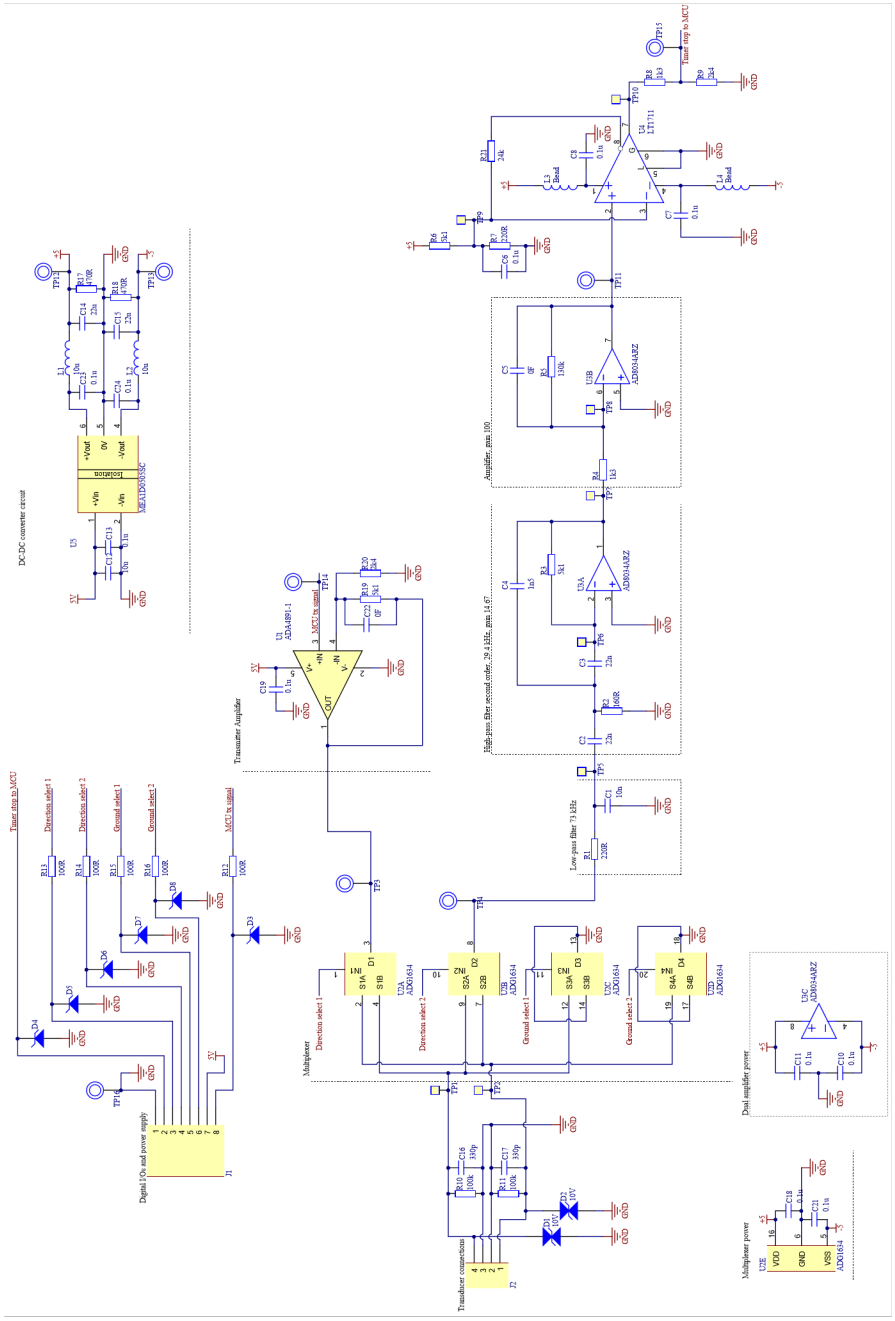

B

Appendix: Reverse-flow results

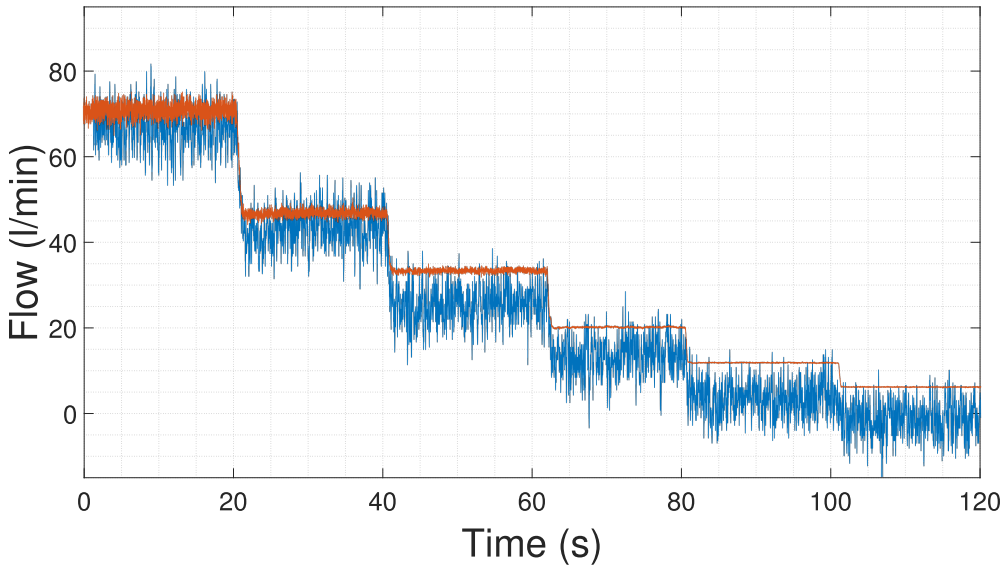

Figure B.1: Flow test with 75 degree transducer angle at 32 mm distance in forward direction.

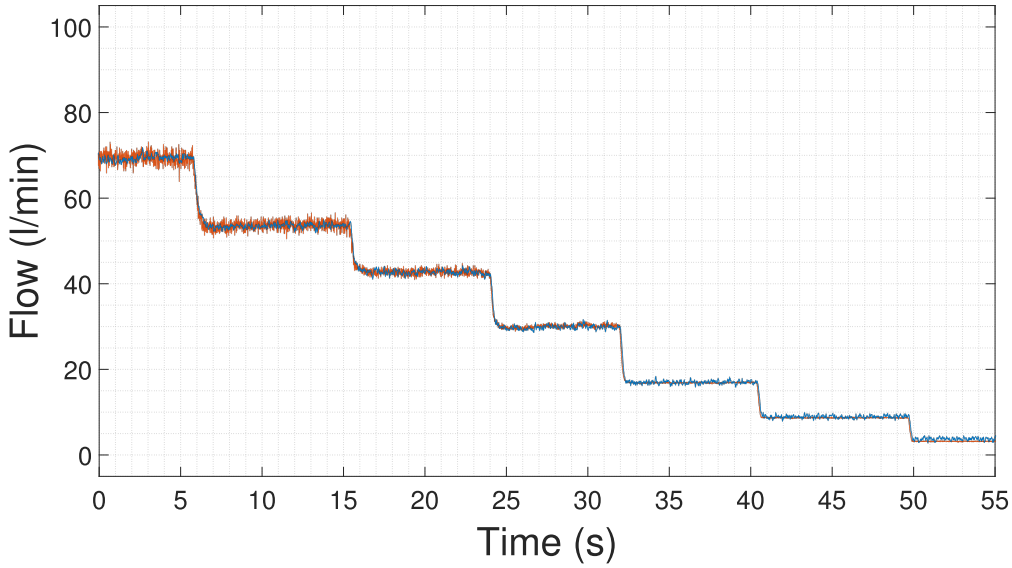

Figure B.2: Flow test with 55 degree transducer angle at 42 mm distance in forward direction.

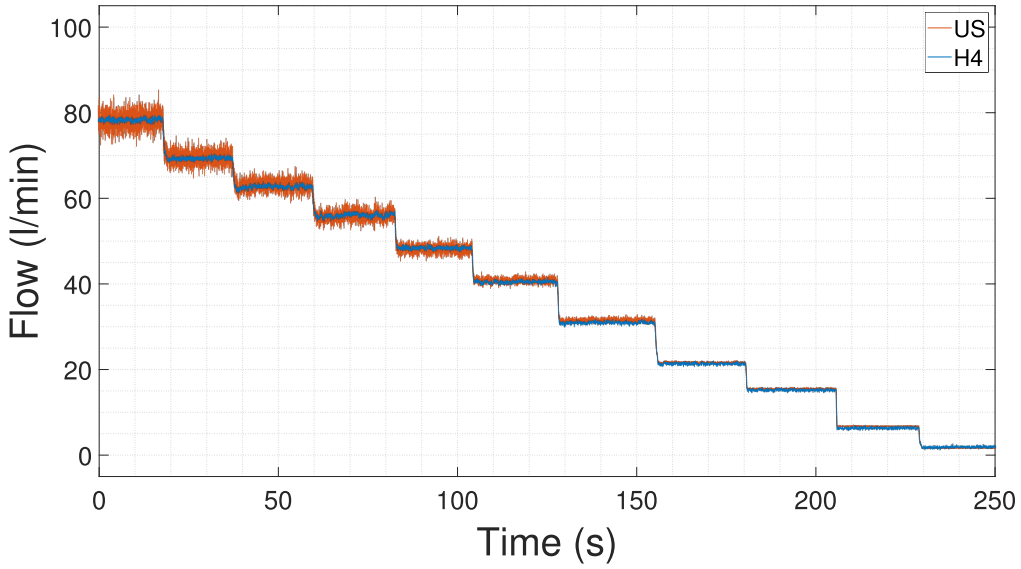

Figure B.3: Flow test with 35 degree transducer angle at 49 mm distance in forward direction.